Dalton Transactions

PERSPECTIVE

View Article Online
View Journal | View Issue

Cite this: *Dalton Trans.*, 2018, **47**, 4408

Comprehensive reaction mechanisms at and near the Ni–Fe active sites of [NiFe] hydrogenases

Hulin Tai, [a,b] Yoshiki Higuchi [b,c] and Shun Hirota *[a,b]

Received 28th December 2017,
Accepted 20th February 2018

DOI: 10.1039/c7dt04910b

rsc.li/dalton

[NiFe] hydrogenase (H_2ase) catalyzes the oxidation of dihydrogen to two protons and two electrons and/or its reverse reaction. For this simple reaction, the enzyme has developed a sophisticated but intricate mechanism with heterolytic cleavage of dihydrogen (or a combination of a hydride and a proton), where its Ni–Fe active site exhibits various redox states. Recently, thermodynamic parameters of the acid–base equilibrium for activation–inactivation, a new intermediate in the catalytic reaction, and new crystal structures of [NiFe] H_2ases have been reported, providing significant insights into the activation–inactivation and catalytic reaction mechanisms of [NiFe] H_2ases. This Perspective provides an overview of the reaction mechanisms of [NiFe] H_2ases based on these new findings.

Introduction

Dihydrogen (H_2) is a potent candidate for a clean energy storage medium. By the oxidation of H_2 in a H_2–O_2 fuel cell, H_2O is produced exergonically, and the released energy is transformed to electricity.[1] The H_2-cleavage reaction plays a key role in H_2 metabolism in various bacteria. Hydrogenase (H_2ase) is a metalloenzyme that catalyses the reversible oxidation of H_2 into two protons and two electrons and/or the reverse reaction.[2–6] Thus, knowledge on the reaction mechanism of H_2ases is beneficial for the design of biocatalysts focused on H_2 generation and biofuel cells.[7–10] H_2ases are classified according to the active site metal contents: [NiFe], [FeFe], and [Fe] H_2ases.[11–13] [NiFe] and [FeFe] H_2ases contain sulphur-bridged bimetallic centers that catalyse the reversible oxidation of H_2, *via* the production of a hydride (H^-): $H_2 \rightleftharpoons H^- + H^+ \rightleftharpoons 2H^+ + 2e^-$, whereas [Fe] H_2ase catalyzes the reduction

[a]*Graduate School of Materials Science, Nara Institute of Science and Technology, 8916-5 Takayama-cho, Ikoma-shi, Nara 630-0192, Japan. E-mail: hirota@ms.naist.jp*
[b]*CREST, Japan Science and Technology Agency, 4-1-8 Honcho, Kawaguchi, Saitama 332-0012, Japan*
[c]*Graduate School of Life Science, University of Hyogo, 3-2-1 Koto, Kamigori-cho, Ako-gun, Hyogo 678-1297, Japan*

Hulin Tai

Hulin Tai is an assistant professor at the Graduate School of Materials Science, Nara Institute of Science and Technology in Japan. He graduated from the College of Chemistry in Jilin University (China) in 2002 and obtained his Ph.D. in chemistry from the University of Tsukuba (Japan) in 2008 under the supervision of Prof. Yasuhiko Yamamoto. He worked at the University of Tsukuba as a research associate and junior assistant professor for five years, before joining the Nara Institute of Science and Technology as an assistant professor in 2013. His research interests are spectroscopic (FT-IR, EPR, NMR) studies of metalloenzymes, metalloproteins, and G-quadruplex DNA.

Yoshiki Higuchi

Yoshiki Higuchi is currently a full professor in the Graduate School of Life Science, University of Hyogo. He obtained his Ph.D. from Osaka University (1984). After a postdoctoral position at the Institute for Protein Research in Osaka University, he was appointed as an assistant professor at the Himeji Institute of Technology (1985). He moved to Kyoto University in 1995 as an associate professor of the Graduate School of Science. In 2002, he moved to the Himeji Institute of Technology (presently University of Hyogo) to become a full professor in the Graduate School of Science. He received the award of The Crystallographic Society of Japan in 1999, 38th Iue Culture Award for Science and Technology in 2014, and Hyogo Science Award in 2017.

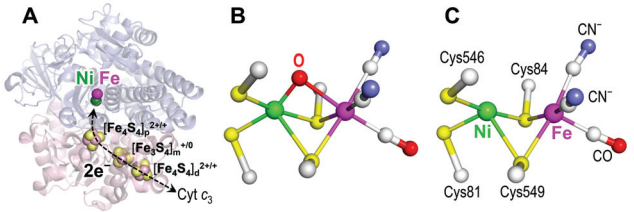

Fig. 1 (A) Overall structure of *Dv*MF [NiFe] H_2ase (in the oxidized state, PDB: 1WUL). The Ni–Fe site and $[Fe_4S_4]_p^{2+/+}$, $[Fe_3S_4]_m^{+/0}$, and $[Fe_4S_4]_d^{2+/+}$ clusters are highlighted. The Ni–Fe site structures of *Dv*MF [NiFe] H_2ase in (B) the oxidized state (Ni-B state, PDB: 1WUJ) and (C) H_2-activated state (PDB: 1WUL). One CO and two CN^- ligands are assigned Fe ligands.[24,31] An additional oxygenic ligand is bridged between the Ni and Fe ions in the oxidized state.[23] Carbon, nitrogen, oxygen, sulphur, nickel, and iron atoms are shown in gray, blue, red, yellow, green, and pink spheres, respectively.

of methenyl-tetrahydromethanopterin (methenyl-H_4MPT^+) with H_2, forming methylene-H_4MPT and H^+.[6,14,15] The catalytic activity of [NiFe] H_2ases usually vanishes in the presence of O_2 (O_2-sensitive, standard), although several [NiFe] H_2ases exhibit catalytic activity in the presence of O_2 (O_2-tolerant).[6–9] The crystal structure of a standard [NiFe] H_2ase from *Desulfovibrio gigas* (*Dg*) at 2.85 Å resolution was reported in 1995,[11] followed by the reports on the structures of standard [NiFe] H_2ases from *Desulfovibrio vulgaris* Miyazaki F (*Dv*MF)[16] and other speices[17–20] with improved resolutions (1.8–2.5 Å), which provided detailed structural information on the Ni–Fe active site. *Dv*MF [NiFe] H_2ase is a periplasmic membrane-attached enzyme comprising two subunits: large (62.5 kDa) and small (28.8 kDa) (Fig. 1A).[16,21–24] The Ni–Fe site is located in the large subunit, and the Ni and Fe ions are bridged with two Cys thiolates (Fig. 1B and C). Other two Cys residues are terminally bound to the Ni ion, whereas one CO and two CN^- ligands are coordinated to the Fe ion.[24–26] An additional oxygenic bridging ligand exists in the oxidized states of [NiFe] H_2ases (Fig. 1B), whereas not in the H_2-activated states (Fig. 1C).[21,23] The Ni site changes its oxidation state (*i.e.* Ni^{3+}, Ni^{2+}, and Ni^+) among various redox states of the enzyme, whereas the Fe site retains a low spin, low oxidation state ($S = 0$, Fe^{2+}).[6] Three Fe–S clusters (proximal $[Fe_4S_4]_p^{2+/+}$, medial $[Fe_3S_4]_m^{+/0}$, and distal $[Fe_4S_4]_d^{2+/+}$) are arranged almost linearly in the small subunit, and mediate the electron transfer between the Ni–Fe site and its physiological redox partner, cytochrome c_3.[27] Three pathways have been proposed for the proton transfer in [NiFe] H_2ase,[24,28,29] whereas four hydrophobic H_2 gas channels have been proposed between the Ni–Fe site and protein surface.[17,30]

Many intermediate states have been identified in the activation–inactivation and catalytic reactions of [NiFe] H_2ases by spectroscopic, X-ray crystallographic, and Ni–Fe site model compound studies.[3–6,10,30,32–38] These states are characterized by electron paramagnetic resonance (EPR) spectroscopy as EPR-active (paramagnetic) and EPR-silent Ni states (Table 1).[5] All states are distinguished by the stretching vibrations of the CO and CN^- ligands at the Fe site in the Fourier transform infrared (FT-IR) spectra.[39] The CO stretching (ν_{CO}) and CN^- stretching (ν_{CN}) IR frequencies, together with the *g*-values, of the characterized states of *Dv*MF [NiFe] H_2ase are listed in Table 1. The EPR-active paramagnetic states are referred to as Ni-A, Ni-B, Ni-C (reduced), Ni-L (light-induced from Ni-C), and Ni-CO (CO-bound Ni-L), whereas the EPR-silent states are referred to as Ni-SU (unready), Ni-SI (Ni-SI_r (ready) and Ni-SI_a (active)), Ni-R (fully reduced), Ni-SCO (CO-bound Ni-SI_a), Ni-SX (highly inactive), and Ni-SL (light-induced from Ni-SX) (Scheme 1).[5,40]

Table 1 CO and CN^- stretching IR frequencies[40–42] and *g*-values[41–43] of the Ni–Fe site of *Dv*MF [NiFe] H_2ase. The IR frequencies at 158 K and *g*-values at 40 K are listed in parentheses, whereas the IR frequencies at 298 K and *g*-values at 163 K are listed without parentheses

	IR frequencies (cm^{-1})				EPR		
State	ν_{CO} (Fe)	ν_{CN} (Fe)		ν_{CO} (Ni)	g_x	g_y	g_z
Ni-A	1956	2085	2094	—	2.32	2.24	2.01
Ni-B	1955	2081	2090	—	2.33	2.16	2.01
Ni-SU	1958	2089	2100	—	—	—	—
Ni-SI_r	1923	2057	2071	—	—	—	—
Ni-SI_a	1943	2074	2086	—	—	—	—
Ni-C	1961	2074	2085	—	2.20	2.14	2.01
Ni-R1	1948	2061	2074	—	—	—	—
Ni-R2	1932	2052	2066	—	—	—	—
Ni-L1	—	—	—	—	2.26	2.11	2.05
Ni-L2	(1911)	(2048)	(2062)	—	2.30	2.12	2.05
Ni-L3	(1890)	(2034)	(2047)	—	(2.32)	—	—
Ni-SX	(1922)	(2061)	(2070)	—	—	—	—
Ni-SL	(1968)	(2076)	(2090)	—	—	—	—
Ni-CO	—	—	—	—	2.13	2.08	2.02
Ni-SCO	1941	2071	2084	2056	—	—	—

Shun Hirota

Shun Hirota is currently a full professor at the Graduate School of Materials Science, Nara Institute of Science and Technology in Japan. He received his Bachelor's and Master's degrees in engineer from Kyoto University in 1990 and 1992, respectively, and gained his Ph. D. from the Graduate University for Advanced Studies in 1995 under the supervision of Prof. Teizo Kitagawa. After working as a JSPS research fellow and post-doctoral researcher in the Institute of Molecular Science at the Okazaki National Research Institutes and in the Department of Chemistry at Emory University, he joined Nagoya University as an assistant professor in 1996, and became an associate professor at Kyoto Pharmaceutical University in 2002. He was invited as a full professor to the Nara Institute of Science and Technology in April 2007. His research interests include structures, functions, and reaction mechanisms of metalloproteins.

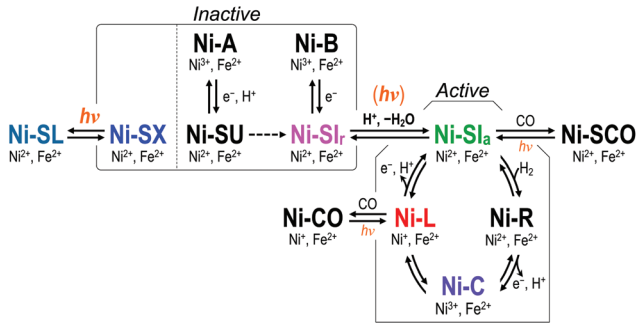

Scheme 1 Reaction scheme of [NiFe] H_2ase.

In this Perspective, we focus on the mechanisms at the Ni–Fe sites of [NiFe] H_2ases for activation–inactivation, catalytic reaction, proton transfer, and O_2-tolerance. Recent developments in crystallographic analyses, spectroscopy techniques, kinetics, and theoretical studies on the enzyme are summarized, together with re-analyses of earlier data, providing an overall view of the [NiFe] H_2ase reaction.

Activation–inactivation mechanism

Aerobically isolated *Dv*MF [NiFe] H_2ase, herein referred to as "as-isolated", is obtained mainly in a paramagnetic Ni-B (Ni^{3+}) state with a minor paramagnetic Ni-A (Ni^{3+}) state and additional EPR-silent inactive Ni^{2+} states (Scheme 1).[30,40,41] Concerning the enzyme activation–inactivation, the acid–base equilibrium between the two EPR-silent Ni-SI_r (Ni^{2+}) and Ni-SI_a (Ni^{2+}) states is recognized as the key reaction (Scheme 1).[6]

Oxidized paramagnetic Ni-A and Ni-B states

The Ni-A and Ni-B states of [NiFe] H_2ase are oxidized states, differing in the time necessary for activation in the presence of H_2 or under electrochemically reducing conditions; the Ni-A state requires a longer time for activation, whereas the Ni-B state is readily activated within seconds.[44–46] To elucidate the origin of the differences in the activation kinetics between the Ni-A and Ni-B states, many spectroscopic and structural investigations have been performed.

The g_x and g_z values of the Ni^{3+} EPR signals between the Ni-A and Ni-B states are very similar, but the g_y values are different (Table 1).[5,47] The IR frequencies of the ν_{CO} and two conjugated ν_{CN} bands of the Ni-A state (ν_{CO}: 1956 cm^{-1}, ν_{CN}: 2085 and 2094 cm^{-1} for *Dv*MF [NiFe] H_2ase) are slightly higher (1–4 cm^{-1}) than the corresponding frequencies of the Ni-B state (ν_{CO}: 1955 cm^{-1}, ν_{CN}: 2081 and 2090 cm^{-1}) (Table 1).[48] The X-ray crystallographic structures of the Ni-A and Ni-B states exhibited additional electron densities at the bridging position between the Ni and Fe ions (Fig. 1B).[19,20,23,49] An oxygen species has been shown to exist at the Ni–Fe site for both oxidized states by EPR experiments using $^{17}O_2$ and $H_2{}^{17}O$.[50,51] The hyperfine splitting in the EPR Ni^{3+} g_z signal of the Ni-B state was resolved faintly, but much better by exchanging the H_2O buffer to D_2O buffer, indicating an exchangeable proton in the vicinity of the Ni–Fe site.[52] According to single crystal electron nuclear double resonance (ENDOR) and hyperfine sublevel correlation (HYSCORE) spectroscopic studies together with DFT mode calculations of *Dv*MF [NiFe] H_2ase, the oxygenic ligand of the Ni-B state has been assigned to a bridging hydroxo (μ-OH^-) ligand.[53,54] For the Ni-A state, the nature of the oxygenic bridging ligand remains contentious;[19,20,23,55,56] however, it has been proposed that an OH^- ligand is bridged at the Ni–Fe site by crystallographic analysis.[49] Single crystal ENDOR experiments of *Dv*MF [NiFe] H_2ase utilizing H/D exchange and DFT simulations supported the hypothesis that a bridging OH^- ligand exists for the Ni-A state, similar to the Ni-B state.[57] However, X-ray crystal structures and theoretical calculations of [NiFe] H_2ases suggest a Cys-sulfoxide (S=O) or a Cys-sulfenic acid (SOH) ligand as a plausible origin for the differences in the activation kinetics of the Ni-A and Ni-B states.[23,46,56,57] A conclusive structural explanation for the differences in the activation kinetics between the Ni-A and Ni-B states requires further experimentation.

EPR-silent Ni-SU and Ni-SI_r states

One-electron reductions of the Ni-A and Ni-B states produce EPR-silent unready Ni-SU (Ni^{2+}) and ready Ni-SI_r states, respectively (Scheme 1).[31,48,58,59] The midpoint potential (E_m) values for the redox transition between the Ni-A and Ni-SU states of *Dv*MF [NiFe] H_2ase are −278 mV at pH 8.2 and −96 mV at pH 5.5.[31,48] Similar pH-dependent E_m values between the Ni-A and Ni-SU states are reported for *Dg* and *Allochromatium vinosum* (*Av*) [NiFe] H_2ases.[58,59] The E_m values change by about −60 mV per pH for the interconversion between the Ni-A and Ni-SU states, in good agreement with a one-proton redox process. The Ni-A state does not react directly with H_2, and thus the reduction of the Ni-A state to the "unready" Ni-SU state is a prerequisite for the reaction.[45,60] The rate-limiting step for the activation from the Ni-SU state to Ni-SI state (Ni-SI_r and Ni-SI_a) is a first order reaction.[58] However, the transition from the Ni-A state to Ni-SU state is reversible at low temperatures (2 °C), whereas that from the Ni-B state to Ni-SI_r state is not.[59] The frequencies of the ν_{CO} and two conjugated ν_{CN} IR bands of the Ni-SU state (ν_{CO}: 1958 cm^{-1}, ν_{CN}: 2089 and 2100 cm^{-1} for *Dv*MF [NiFe] H_2ase) are slightly higher than the corresponding frequencies of the Ni-A state (ν_{CO}: 1956 cm^{-1}, ν_{CN}: 2085 and 2094 cm^{-1}), whereas the frequencies of the Ni-SI_r state (ν_{CO}: 1923 cm^{-1}, ν_{CN}: 2057 and 2071 cm^{-1}) are 19–32 cm^{-1} lower than the corresponding frequencies of the Ni-B state (ν_{CO}: 1955 cm^{-1}, ν_{CN}: 2081 and 2090 cm^{-1}) (Table 1).[48] The existence of various inactive states, including the Ni-SU and Ni-SI_r states, may be relevant to the effective storage of [NiFe] H_2ases, although an exquisite mechanism for the activation of the inactive states is necessary.

Activation–inactivation mechanism of the acid–base equilibrium between the Ni-SI_r and Ni-SI_a states

The Ni-SI_r state is activated to another EPR-silent state, Ni-SI_a, by protonation at the Ni–Fe site (Scheme 1).[31,58,59] The E_m

values between the Ni-B and Ni-SI ($Ni\text{-}SI_r$ and $Ni\text{-}SI_a$) states of *Dg*, *Av*, and *Dv*MF [NiFe] H_2ases are −40 to −60 mV per pH,[31,58,59] indicating the involvement of one proton in the Ni-B ↔ $Ni\text{-}SI_a$ transition. The acid–base equilibrium between the two Ni-SI states is a common feature among [NiFe] H_2ases, and the equilibrium has been identified as the key reaction for the enzyme activation–inactivation.[6] The acid–base equilibrium exhibits a pK_a value of about 8 for various [NiFe] H_2ases.[31,58,59] Mainly two mechanisms have been proposed to explain the equilibrium. In the first mechanism, the bridging OH^- ligand exists in the $Ni\text{-}SI_r$ state, and the OH^- ligand leaves the Ni–Fe site as a H_2O molecule by protonation, producing the $Ni\text{-}SI_a$ state (Fig. 2, Mechanism 1).[3,45,59,61] In the second mechanism, the $Ni\text{-}SI_r$ state accepts a proton at the terminal Ni^{2+}-coordinating Cys side chain that acts as a proton accepting base, where the bridging ligand in the $Ni\text{-}SI_r$ state remains contentious (Fig. 2, Mechanism 2).[62–64]

We found that the $Ni\text{-}SI_r$ state of *Dv*MF [NiFe] H_2ase is photo-activated to the $Ni\text{-}SI_a$ state by Ar^+ laser irradiation at 514.5 nm (Fig. 3A).[40] Low-temperature (103–238 K) conditions have been used to trap intermediates and non-equilibrium states. Phenosafranine-oxidized *Dv*MF [NiFe] H_2ase was obtained by partial oxidation of the H_2-activated enzyme with an anaerobic addition of 5 equivalents of phenosafranine. In the difference (light-minus-before) FT-IR spectra of phenosafranine-oxidized *Dv*MF [NiFe] H_2ase between the spectra during and before light irradiation at 178–203 K at pH 8.0, we observed positive IR bands assignable to the $Ni\text{-}SI_a$ state (ν_{CO}: 1944 cm^{-1}, ν_{CN}: 2077 and 2089 cm^{-1}) and negative bands assignable to the $Ni\text{-}SI_r$ state (ν_{CO}: 1924 cm^{-1}, ν_{CN}: 2056 and 2071 cm^{-1}) (Fig. 3A and Table 1). The positive and negative bands are related to the light-induced product and light-sensitive reactant, respectively, and thus the difference spectra show that the $Ni\text{-}SI_r$ state is photo-activated to the $Ni\text{-}SI_a$ state. Notably, the light-induced conversion of the $Ni\text{-}SI_r$ state to $Ni\text{-}SI_a$ state decreased significantly at pH 9.6, indicating that protonation is involved in the conversion. After the $Ni\text{-}SI_r$-to-$Ni\text{-}SI_a$ photo-activation, reconversions of the $Ni\text{-}SI_a$ state to $Ni\text{-}SI_r$ state at 183–203 K followed first-order kinetics.[65] Large activation energy values (61 ± 2 kJ mol^{-1} at pH 8.0 and 67 ± 2 kJ mol^{-1} at pD 8.0) and a large kinetic isotope effect (k_H/k_D = about 150 at 203 K) were determined for the reconversion from the Arrhenius plot analysis (Fig. 4). For a simple S–H bond cleavage, such as deprotonation of the Ni^{2+}-coordinating Cys residue, the k_H/k_D value at 203 K is about 10, which is estimated from the difference in the zero-point energies of the S–H and S–D bonds (about 3.9 kJ mol^{-1}), and thus, the large k_H/k_D value for the conversion of the $Ni\text{-}SI_a$ state to $Ni\text{-}SI_r$ state is unexplainable with a simple S–H bond cleavage.[66] Additionally, the conversions at 173–203 K were about 10 times faster at pH 8.5 compared to those at pH 8.0 (Fig. 4), where the increase was caused by the increase in the activation entropy ($\Delta S^{\ddagger}$) value of about 3 times.[65] These results indicate that the conversion of the $Ni\text{-}SI_a$ state to $Ni\text{-}SI_r$ state is an intricate reaction, supporting Mechanism 1, in which the conversion of the $Ni\text{-}SI_a$ state to $Ni\text{-}SI_r$ state includes the insertion of the bridging OH^- ligand

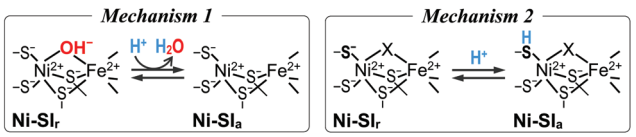

Fig. 2 The two proposed mechanisms for the acid–base equilibrium between the $Ni\text{-}SI_r$ and $Ni\text{-}SI_a$ states. X may be OH^-, H_2O, or empty.[62–64] Adapted with permission from ref. 65. Copyright 2017 Royal Society of Chemistry.

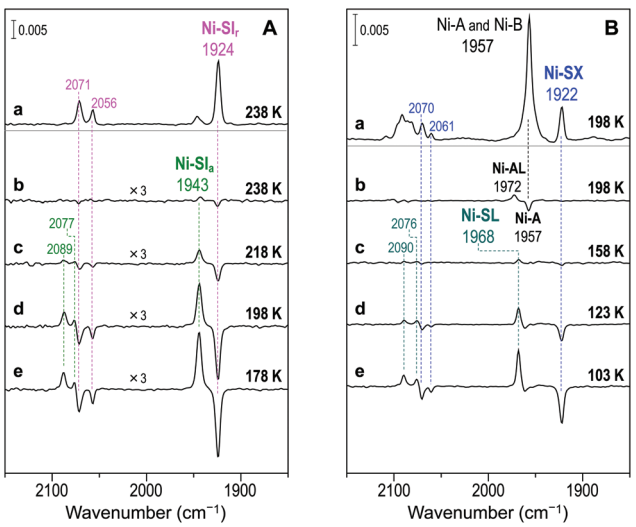

Fig. 3 FT-IR spectra of (A) phenosafranine-oxidized and (B) as-isolated *Dv*MF [NiFe] H_2ase at 178–238 and 103–198 K, respectively, under N_2 atmospheres at pH 8.0. (a) FT-IR spectra before light irradiation and (b–e) light-minus-before difference spectra between the spectra during and before light irradiation are shown. The difference spectra of the phenosafranine-oxidized enzyme are expanded by three. Adapted with permission from ref. 40. Copyright 2016 Royal Society of Chemistry.

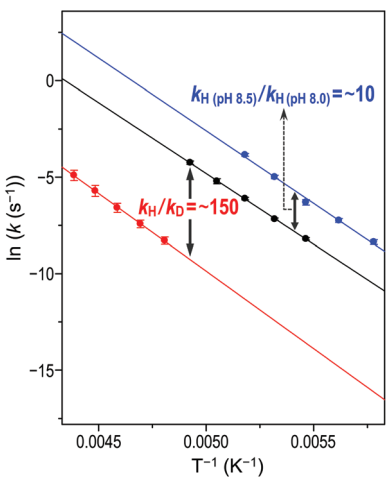

Fig. 4 Arrhenius plots for the conversion of the $Ni\text{-}SI_a$ state to $Ni\text{-}SI_r$ state of *Dv*MF [NiFe] H_2ase at pH 8.0 (black), pH 8.5 (blue), and pD 8.0 (red). Adapted with permission from ref. 65. Copyright 2017 Royal Society of Chemistry.

by the incorporation of a H_2O molecule into the Ni–Fe site and subsequent deprotonation (Fig. 2). It has been clarified that not only a simple proton transfer is involved in the transition between the Ni-SI_r and Ni-SI_a states; however, further studies are necessary to elucidate the mechanism, including the large isotope effect for the conversions of the Ni-SI_a state to Ni-SI_r state.

A newly identified EPR-silent highly inactive state

A light-sensitive EPR-silent state photo-converts to an EPR-silent Ni-SL (Ni^{3+}) state in the as-isolated *Dv*MF [NiFe] H_2ase; however, the light-sensitive state was previously misassigned to the Ni-SI_r state.[40,67] In fact, the frequencies of the light-sensitive state (ν_{CO}: 1922 cm^{-1}, ν_{CN}: 2061 and 2070 cm^{-1} for the *Dv*MF [NiFe] H_2ase) are 1–5 cm^{-1} different from the corresponding frequencies of the Ni-SI_r state (ν_{CO}: 1924 cm^{-1}, ν_{CN}: 2056 and 2071 cm^{-1}) (Fig. 3B and Table 1).[40] These frequency differences indicate that the light-sensitive state is different from the Ni-SI_r state; this newly identified light-sensitive state is named Ni-SX in Scheme 1.

The Ni-SX (Ni^{2+}) state did not convert to the Ni-SI_a state through the acid–base equilibrium, supporting the hypothesis that the Ni-SX state is different from the Ni-SI_r state and demonstrating that it is not a ready state.[40] A certain amount of *Dv*MF [NiFe] H_2ase is still in the Ni-SX state after the treatment of the as-isolated enzyme with dithionite, although it is activated slowly by H_2 (time constant of about 50 min), revealing that the Ni-SX state is highly inactive. The Ni-SX state is not produced by the air-oxidation of the H_2-activated *Dv*MF [NiFe] H_2ase or after the dithionite reduction of the air-oxidized enzyme. These results indicate that although the as-isolated enzyme contains the Ni-SX state, the Ni-SX state is not formed *in vitro* during the generation or activation of the Ni-A and Ni-B states. For [NiFe] H_2ases from sulphur-metabolizing bacterium *Av* and *Desulfovibrio fructosorans* (*Df*), an inactive state (Ni-'S_{ox}') similar to the Ni-SX state exists.[49,59] The ν_{CO} and ν_{CN} frequencies of the Ni-'S_{ox}' state for *Df* [NiFe] H_2ase (ν_{CO}: 1911, ν_{CN}: 2059 and 2068 cm^{-1}) are 1–5 cm^{-1} lower than the corresponding frequencies of its Ni-SI_r state (ν_{CO}: 1913 cm^{-1}, ν_{CN}: 2054 and 2069 cm^{-1});[49,68] the frequency character of the Ni-'S_{ox}' state being similar to that of the Ni-SX state of *Dv*MF [NiFe] H_2ase. The Ni-'S_{ox}' state is proposed to possess a terminal Ni-coordinating Cys-persulfide ligand at the Ni–Fe site by X-ray crystallographic analysis.[49] The Ni-SX state of *Dv*MF [NiFe] H_2ase may be similar to the Ni-'S_{ox}' state of *Df* [NiFe] H_2ase, and the required reduction of the persulfide bond may explain the extremely slow activation of the Ni-SX state. The elucidation of the nature of this newly identified Ni-SX state may help clarify the activation–inactivation mechanism of [NiFe] H_2ase.

Catalytic reaction mechanism

The Ni-SI_a, Ni-C, and Ni-R states have been reported to be involved in the catalytic cycle of [NiFe] H_2ase,[58,69] while we and other groups recently showed that the Ni-L state is also involved in the catalytic cycle (Scheme 2).[70–73] These states convert among each other by the addition or release of electrons, protons, and H_2.[3–6,30,58,69–74]

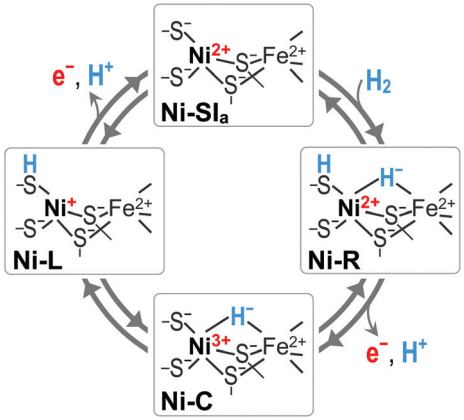

Scheme 2 Proposed catalytic cycle of [NiFe] H_2ase.

Ni-SI_a ↔ Ni-R transition

The Ni-SI_a, Ni-C, and Ni-R states are the main states that have been observed in the catalytic cycle under physiologically relevant conditions for standard [NiFe] H_2ases. According to FT-IR studies, the Ni-SI_a state reacts with CO, resulting in the formation of an EPR-silent Ni-SCO (Ni^{2+}) state (Scheme 1).[41,68] Although CO does not bind to the Ni-A/SU, Ni-B/SI_r, Ni-C, and Ni-R states, it binds to the Ni-SI_a state, since in this state the non-protein bridging ligand that blocks the access of CO to the Ni–Fe site is absent.[41] At temperatures below 120 K, the photo-dissociation of the extrinsic CO ligand from [NiFe] H_2ase in the Ni-SCO state results in the enzyme in the Ni-SI_a state.[41,75] According to high-resolution (1.2 Å) X-ray crystal structures and resonance Raman spectra of the Ni-SCO state of *Dv*MF [NiFe] H_2ase, the extrinsic CO ligand is bound to the Ni atom in a slightly bent conformation.[22] Interestingly, the electron density peak of the extrinsic CO ligand disappeared with no new peak at the Ni–Fe bridging position upon the illumination of the Ni-SCO state with strong white light at 100 K, indicating that the OH^--bridging ligand position (in the oxidized enzyme) at the Ni–Fe site is unoccupied in the Ni-SI_a state.[22]

When the Ni-SI_a state of [NiFe] H_2ase reacts with H_2 in the first step of the catalytic cycle of H_2 oxidation, H_2 is cleaved heterolytically, resulting in the fully reduced Ni-R (Ni^{2+}) state with a bridging hydride (H^-) ligand at the Ni–Fe site.[32,45,61,76,77] Direct evidence for the bridging H^- ligand in the Ni-R state was provided first by the ultrahigh resolution (0.89 Å) X-ray structure of the anaerobically isolated *Dv*MF [NiFe] H_2ase reported by Ogata *et al.*[24] H^- at the Ni–Fe bridge and a proton bound to the sulfur atom of the Ni-coordinating Cys546 ligand (*Dv*MF sequence) were observed in the X-ray crystal structure, supporting the hypothesis that Cys546 is the initial proton accepting base for the heterolytic cleavage of H_2 (Fig. 5). A shortened Ni–H^- distance (1.58 Å) relative to the

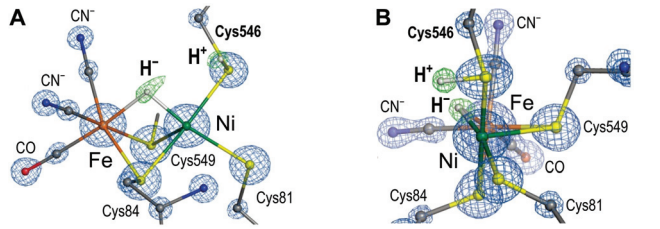

Fig. 5 X-ray crystallographic structural evidence for a bridging H^- and protonation of the Cys546 side chain in the Ni-R state of *Dv*MF [NiFe] H_2ase. The $2F_o-F_c$ electron density maps of the Ni-R state at (A) 0.89 Å and (B) 1.06 Å resolutions are shown in blue and green, respectively. Adapted with permission from ref. 24. Copyright 2015 Nature Publishing Group.

Fe–H^- distance (1.78 Å) indicated a tighter binding of H^- to the Ni atom compared to the Fe iron in the Ni-R state. The existence of the bridging H^- ligand in the Ni-R state was supported by nuclear resonance vibrational spectroscopy, where the frequency of the Ni–H^-–Fe 'wagging' vibrational mode at 675 cm^{-1} was sensitive to the H/D isotope effect, and DFT calculations indicated a low-spin Ni–H^-–Fe core in the Ni-R state with the Ni–H^- bond being stronger than the Fe–H^- bond.[78,79] However, these results are inconsistent with the Ni-R state synthetic model compound structures, in which the H^- ligand is either displaced toward or terminally bound to the Fe atom.[77,80–84] Additionally, DFT calculations on a [NiFe] model complex suggest an Fe-centered reactivity rather than a Ni-centered reactivity for the proton reduction catalysis.[85]

Evans *et al.* reported an alternative mechanism for the conversion of the Ni-SI_a state to Ni-R state of [NiFe] H_2ase from *Escherichia coli* (*Ec*).[86] An Arg residue (Arg509 in the *Ec* sequence) was suggested as a general proton accepting base for the H_2 heterolytic cleavage (Fig. 6). Arg509 is highly conserved in [NiFe] H_2ases, and its strong basic guanidinium group (pK_a = about 13.8)[87] sits only 4.5 Å away from the Ni atom. The R509K mutant (substitution of Arg509 to Lys) exhibits >100-fold lower H_2 oxidation activity than that of the wild type enzyme (Fig. 6A), despite the inner coordination sphere structure of the Ni–Fe site being virtually unchanged. The D574N and D118A mutants (substitution of Asp to Asn and Ala, respectively), in which the position of the guanidine group of Arg509 was retained, showed 80% and 26% activity, respectively, compared to that of the wild-type enzyme, indicating that the suspended guanidine group of the Arg residue near the Ni–Fe site is essential for the H_2-catalysis (Fig. 6B). This mechanism is similar to that of [FeFe] H_2ase, where the pendant amine groups of the azadithiolate bridging ligand act as initial proton acceptors for H_2 oxidation.[88] However, this Arg proton accepting mechanism is difficult to reconcile with the putative thiol-based proton location proposed by others for the Ni-R state,[24,32,89–95] and further investigation is necessary to eliminate the contradiction.

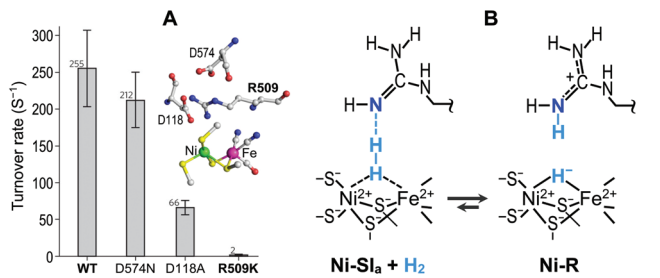

Fig. 6 (A) Comparison of the H_2 oxidation activities among wild-type and various mutants of *Ec* [NiFe] H_2ase. X-ray crystal structure of the wild-type enzyme (PDF: 5A4M), exhibiting a guanidium group of R509 positioned above the Ni–Fe site. Carbon, nitrogen, oxygen, sulphur, nickel, and iron atoms are shown in gray, blue, red, yellow, green, and pink spheres, respectively. (B) Proposed mechanism for the heterolytic cleavage of H_2, based on a frustrated Lewis pair *via* the guanidium side chain of the conserved Arg residue. Adapted with permission from ref. 86. Copyright Nature Publishing Group.

Ni-R ↔ Ni-C transition

The paramagnetic Ni-C (Ni^{3+}) state is generated by one-electron oxidation of the Ni-R state.[31,58,59] ENDOR spectroscopic studies revealed an exceptionally strong ^1H hyperfine interaction of an exchangeable hydrogen species in the Ni-C states of *Dg*[96] and *Thiocapsa roseopersicina*[97] [NiFe] H_2ases, and theoretical calculations predicted the bridging ligand of the Ni-C state as H^-.[90,98–100] Lubitz and co-workers more completely determined the hyperfine coupling tensor components of the strongly coupled hydrogen species by ENDOR and HYSCORE spectroscopy for the Ni-C states of *Dv*MF[101] and *Ralstonia eutropha* (*Re*)[102] [NiFe] H_2ases using H/D exchange, uniquely identifying the H^- ligand in the bridging position. The bridging H^- location is in good agreement with those obtained by DFT calculations on the Ni-C state models.[101,102]

The E_m values between the Ni-C and Ni-R states of *Dv*MF [NiFe] H_2ase are pH-dependent (about −60 mV per pH), indicating the dissociation of a proton for the transition from the Ni-R state to Ni-C state.[31] Five anionic ligands surrounding the Ni site play a role in stabilizing the oxidized Ni^{3+} state, and may result in the terminal Cys ligands (Cys546 and Cys81 in the *Dv*MF sequence) being deprotonated in the Ni-C state, in contrast to the Ni-R state.[38,63] By time-resolved IR spectroscopy utilizing the photo-triggered chemical potential jump approach, Greene *et al.* reported a stepwise electron transfer (ET)–proton transfer (PT) kinetics for the conversion of the Ni-C state to Ni-R state with time scales faster than the turnover frequency in [NiFe] H_2ase from *Pyrococcus furiosus* (*Pf*) (Fig. 7).[72] The pH-dependent ET–PT kinetics indicated that the PT process is slowed at pH > 7, which is close to the pK_a (about 6.8, estimated from the pH-dependent FT-IR spectra of the Ni-C state)[103] of Glu17 (in the *Pf* sequence; corresponding to Glu34 in *Dv*MF [NiFe] H_2ase) near the Ni–Fe site.[104] Although this Glu residue is in close vicinity to the terminal Ni-coordinating Cys ligand (Cys546 in the *Dv*MF sequence), the ET process is unaffected by pH (pH 6.3–7.7), providing additional evidence that the proton is supplied from the Glu residue for this step.[72,105]

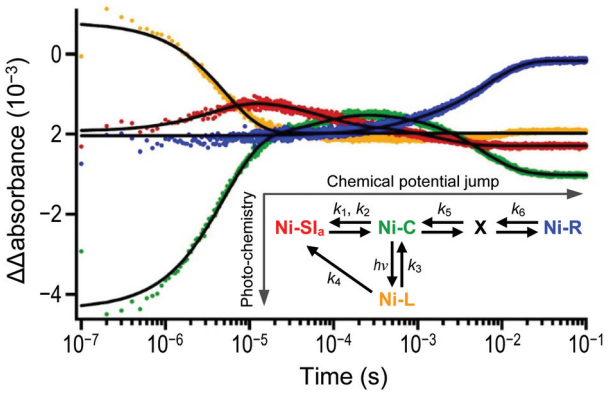

Fig. 7 Transient IR data of *Pf* [NiFe] H_2ase. Color scheme: Ni-SI_a (1948 cm^{-1}), red; Ni-C (1967 cm^{-1}), green; Ni-L (1920 cm^{-1}), orange; Ni-R (1954 cm^{-1}), blue; global fits, black. Adapted with permission from ref. 72. Copyright 2015 American Chemical Society.

Ni-C ↔ Ni-SI_a transition

The final oxidation and deprotonation step in the catalytic cycle of [NiFe] H_2ase, *i.e.*, the transition from the Ni-C state to Ni-SI_a state (E_m = −247 mV at pH 5.4 for *Dv*MF [NiFe] H_2ase[31]), and the regulation of the cycle have been revealed recently.[6,105,106] The catalytic Ni-C state is light sensitive and photo-converts to a number of Ni-L states (Ni-L1, Ni-L2, and Ni-L3), which can be observed at cryogenic temperatures.[6] The Ni-L states possess a d^9 Ni^+ paramagnetic electron configuration; these states were initially identified *via* EPR spectroscopy for [NiFe] H_2ase from *Chromatium vinosum* (*Cv*)[107] and later for other [NiFe] H_2ases.[43,101,102,108–116] The Ni-L1 state is an unstable transient state, whereas the Ni-L2 state is the most prominent Ni-L state at 60 K.[43,108–110] The intensity of the EPR signals of the Ni-L1 state increases when the temperature is decreased from 60 K to 30 K after 6 min of light irradiation, whereas rapid conversion of the Ni-L1 state to the Ni-L2 state is induced by increasing the temperature from 30 K to 60 K after light irradiation.[108,109] The Ni-L1 and Ni-L2 states convert to the Ni-L3 state by extensive light irradiation.[109] The bridging H^- ligand dissociates from the Ni–Fe site and is oxidized to a proton by the conversion of the Ni-C state to Ni-L states, according to ENDOR and HYSCORE studies together with theoretical calculations.[101,102] According to DFT calculations, the Ni^+ and Fe^{2+} ions form a Ni–Fe metal–metal bond in the Ni-L state, as well as in the Ni-SI_a state, where both states possess a vacant bridging ligand position at the Ni–Fe site.[117] The formation of the Ni–Fe bond is relevant for the stabilization of the states with a vacant bridging Ni–Fe site. Although the Ni-L states have been mentioned by theoretical studies as additional intermediates during the transition from the Ni-C state to Ni-SI_a state,[69,92,99,118,119] the Ni-L states have been thought to be artifacts due to illumination at cryogenic temperatures required for the formation of the NI-L states from the Ni-C state.

We provided the first experimental evidence supporting the hypothesis that the Ni-L state is a catalytic intermediate.[70] Low-temperature light irradiation to the Ni-C state resulted in

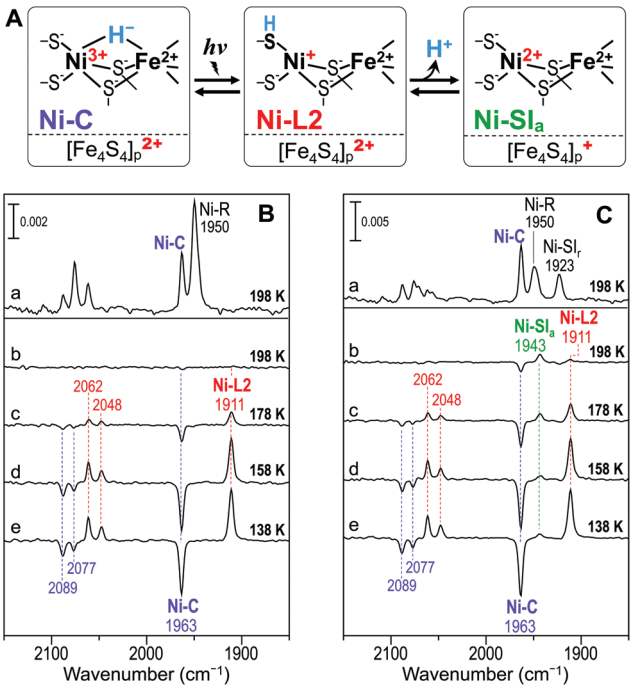

Fig. 8 Light-induced interconversion between the Ni-C, Ni-L, and Ni-SI_a states. (A) Reaction scheme showing that the conversion of the Ni-L state to Ni-SI_a state occurs when the proximal $[Fe_4S_4]_p^{2+/+}$ cluster is oxidized and can accept an electron. (B, C) FT-IR spectra of H_2-activated *Dv*MF [NiFe] H_2ase under (B) H_2 and (C) N_2 atmospheres at 138–198 K: (a) FT-IR spectra before light irradiation; (b–e) light-minus-before difference FT-IR spectra between the spectra during and before light irradiation. Adapted with permission from ref. 70. Copyright 2014 Wiley-VCH.

a relatively large amount of the Ni-SI_a state when the proximal $[Fe_4S_4]_p$ cluster was oxidized and could accept an electron from the Ni–Fe site (Fig. 8A). Positive FT-IR bands assigned to the Ni-L2 state (ν_{CO}: 1911 cm^{-1}, ν_{CN}: 2048 and 2062 cm^{-1}) and negative bands assigned to the Ni-C state (ν_{CO}: 1963 cm^{-1}, ν_{CN}: 2077 and 2089 cm^{-1}) were observed in the light-minus-before difference FT-IR spectra of H_2-actiavted *Dv*MF [NiFe] H_2ase at pH 8.0 at 138–198 K under an H_2 atmosphere (Fig. 8B and Table 1). Interestingly, under an N_2 atmosphere, in addition to the positive Ni-L2 state bands, a positive ν_{CO} band (1943 cm^{-1}) assignable to the Ni-SI_a state was observed in the light-minus-before difference spectra, indicating that the Ni-C state also converts to the Ni-SI_a state by light-irradiation (Fig. 8C). The amount of the Ni-C state converting to the Ni-L state decreased at higher temperatures, whereas that converting to the Ni-SI_a state increased. These results provide strong evidence for the Ni-L state being kinetically trapped at 138 K and is an intermediate for the conversion of the Ni-C state to Ni-SI_a state. The difference in the light-minus-before difference FT-IR spectra between under H_2 and N_2 atmospheres is attributed to the difference in the redox state of the proximal $[Fe_4S_4]_p^{2+/+}$ cluster. All $[Fe_4S_4]_p$ clusters in the Ni-C state are reduced ($[Fe_4S_4]_p^+$) and spin–spin couple with the Ni^{3+} center under an H_2 atmosphere, according to EPR measurements. Under an N_2 atmosphere, about 15% of the $[Fe_4S_4]_p$ clusters in the Ni-C

state are oxidized ($[Fe_4S_4]_P^{2+}$); the amount of the oxidized $[Fe_4S_4]_P^{2+}$ clusters corresponds well to the percentage (about 14%) of the Ni-C state photo-converting to the Ni-SI_a state estimated by FT-IR measurements. These results indicate that the redox state of the proximal $[Fe_4S_4]_P^{2+/+}$ cluster may control the transition of the Ni-L state to Ni-SI_a state. The transition of the Ni-L state to Ni-SI_a state produces a proton and an electron, and the produced electron may be transferred to the proximal $[Fe_4S_4]_P$ cluster. When the $[Fe_4S_4]_P$ cluster is in the reduced state ($[Fe_4S_4]_P^{+}$), it cannot receive an electron, and thus the transition of the Ni-L state to Ni-SI_a state is inhibited. These results suggest a specific electron pathway through the $[Fe_4S_4]_P$ cluster during the conversion of the Ni-L state to Ni-SI_a state, and the pathway is gated by the oxidation state of the $[Fe_4S_4]_P$ cluster (Fig. 8A). Brazzolotto *et al.* reported the bimetallic [NiFe] compound that represented the Ni-L and Ni-R states and displayed a high H_2 oxidation activity (second-order rate constant, 2.5×10^4 M^{-1} s^{-1}; turnover frequency, 250 s^{-1}), supporting the hypothesis that the Ni-L state is an intermediate of the catalytic cycle.[120]

The O_2-tolerant [NiFe] H_2ase from *Aquifex aeolicus* (*Aa*) exhibited mainly the Ni-L signals in the EPR spectrum by incubation under an H_2 atmosphere for several hours under normal room light, *i.e.*, free from strong light.[121] H^- is bound weaker to the Ni–Fe site in the Ni-C state of *Aa* [NiFe] H_2ase compared to H^- bound in standard [NiFe] H_2ases.[114] The weaker binding of H^- to the Ni–Fe site for *Aa* [NiFe] H_2ase is consistent with the stronger light sensitivity of the Ni-C state, greater lability of the H^- complex, and higher catalytic redox potential of bio-H_2 oxidation for *Aa* [NiFe] H_2ase compared to those for standard [NiFe] H_2ases. By using a protein film electrochemical approach combined with IR spectroscopy, Hidalgo *et al.* showed that the Ni-L state of O_2-tolerant *Ec* [NiFe] H_2ase forms reversibly in response to the steady-state H_2 oxidation, strongly supporting the hypothesis that the Ni-L state is a catalytic intermediate (Fig. 9).[71] Under an Ar atmosphere, two Ni-R states were dominant, while two Ni-L states (and the Ni-C state) were observable at −594 V, at which there was no detectable catalytic turnover (Fig. 9B). The population of the Ni-R states decreased as the potential was stepped up to −199 V, while that of the Ni-L states (and the Ni-C and Ni-SI_a states) increased. These spectra represent the first room-temperature observation of the Ni-L states in the dark without using UV/vis light. The populations of the Ni-R, Ni-C, and Ni-L states decreased as the potential was stepped up further to −0.074 V, where the Ni-SI_a state became the dominant state. At the most positive applied potential (+0.356 V), only the Ni-B state was detected. Under an H_2 atmosphere, no obvious difference was observed in the IR spectrum from that under an Ar atmosphere at −594 V (Fig. 9C). However, at more positive potentials, where *Ec* [NiFe] H_2ase engages in electrocatalysis, significant differences in the distribution of the states were observed compared to the spectra under an Ar atmosphere. At intermediate potentials (−0.199 and −0.074 V), the higher and lower populations of the Ni-R and Ni-SI_a states, respectively, were consistent with the fast attack of H_2 to the Ni-SI_a state. The observation of the Ni-L and Ni-C states at the highest potential of +0.356 V, outside the potential window where the states are observed under non-turnover conditions, provides strong evidence that both Ni-L and Ni-C states are generated in response to the catalytic H_2 oxidation. The populations of the Ni-L and Ni-C states remained in the same ratio at all potentials for measurements, as observed under an Ar atmosphere, supporting a potential-independent equilibrium between these two states. Additionally, under the conditions of catalytic H_2 oxidation, the total population of the Ni-L and Ni-C states remained constant. These results suggest that the formation rate of the Ni-C state from Ni-R state is similar to the conversion rate of the Ni-L state to Ni-SI_a state, and that the electron and proton transfer rates in both reactions exhibit similar potential dependences. Murphy *et al.* demonstrated a pH-dependent proton migration on the reversible conversion of the Ni-C and Ni-L states for *Ec* [NiFe] H_2ase, where the conversion proceeds readily in the dark at ambient temperature, and the Ni-C and Ni-L states share the same potential dependence over pH 3.0–8.0.[73] The proximal Fe–S cluster of *Ec* [NiFe] H_2ase exhibits unusually high redox potentials ($[Fe_4S_3]_P^{5+/4+/3+}$, +230 mV and +30 mV),[122] which are more positive than the redox potential of its Ni-L/Ni-SI_a transition at all pH values. The $[Fe_4S_3]_P$ cluster is thus predominant in the most reduced state ($[Fe_4S_3]_P^{3+}$), consistent with the inhibition of the electron transfer from the Ni–Fe site to the $[Fe_4S_3]_P$ cluster during the conversion of the Ni-L state to Ni-SI_a state, and the resulting readiness of the Ni-L state formation for *Ec* [NiFe] H_2ase.

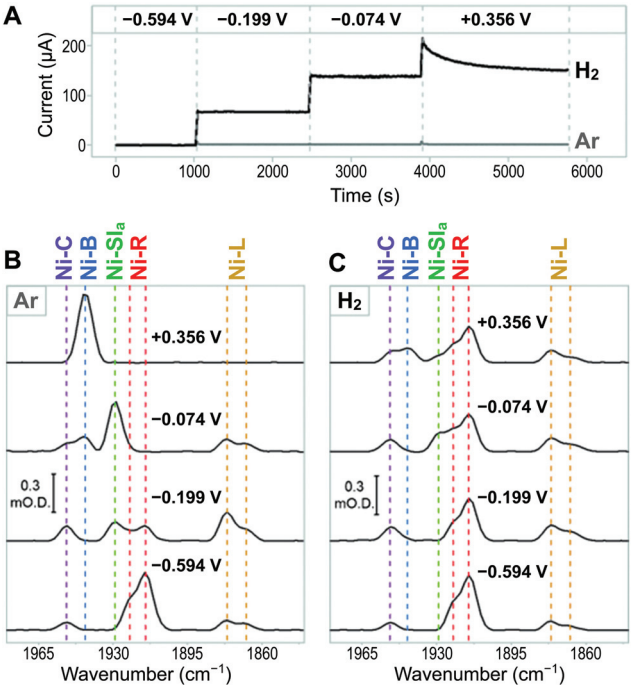

Fig. 9 (A) Current–time traces of *Ec* [NiFe] H_2ase in Ar- and H_2-saturated solutions. (B, C) FT-IR spectra of *Ec* [NiFe] H_2ase in the region at each potential under (B) Ar and (C) H_2 atmospheres. Adapted with permission from ref. 71. Copyright 2015 Wiley-VCH.

The direct and reversible formation of the Ni-SI_a state from two Ni-L states on the subturnover frequency time scales has been demonstrated by time-resolved IR spectroscopy at room temperature (Fig. 7).[72] After light irradiation (lag time < 10^{-7} s), significant Ni-C state bleaching was observed, similar to cryogenic photolysis studies,[42,70] where two Ni-L states were observed. Interestingly, during the reconversion of the Ni-L state to Ni-C state, some of the Ni-SI_a states were observed on a 10^{-7}–10^{-5} s time scale, demonstrating that the Ni-L state may convert to the Ni-C or Ni-SI_a state. The reduction dynamics observed on later time scales (10^{-5}–10^{-3} s) indicated that the loss of the Ni-SI_a state was concomitant with the formation of the Ni-C state. A global kinetic analysis of the data suggested a serial mechanism for the reaction of the Ni-L state: a proton coupled electron transfer (PCET) reaction for the transition of the Ni-SI_a state to Ni-L state and subsequent rapid relaxation to the Ni-C state.

A H_2-binding Ni-SI_a state, herein termed Ni-SI–H_2, has been proposed in the catalytic mechanism of H_2-reduction/H^+-oxidation.[72] Computational studies on [NiFe] H_2ase models support the hypothesis that the binding of H_2 to Ni is more favorable than that to Fe.[91,123,124] However, the initial H_2-binding site in the Ni-SI–H_2 state has not been established, and the complete determination of the catalytic reaction mechanism at the Ni–Fe site of [NiFe] H_2ases would be a promising subject for further studies.

Proton transfer between the Ni–Fe site and protein environment

The proton transfer pathways in [NiFe] H_2ases are presumably well organized, since the H_2 oxidation at the Ni–Fe site is considerably high (turnover frequency >10^3 s^{-1}).[106] The proton acceptor during the conversion of the Ni-C state to Ni-L state is proposed by theoretical[117] and Raman studies;[115,116] the proton is transferred from the Ni–Fe site to the Ni-coordinating terminal Cys ligand (Cys546 in the *Dv*MF sequence) that is located close to the putative proton transfer pathway.[24,28–30] Higher temperature factors in the X-ray crystallographic structures of [NiFe] H_2ases have been observed for the Ni-coordinating sulfur atom of the terminal Cys ligand (Cys546 for *Dv*MF[21,22,24] and Cys530 for *Dg*[11]) compared to those of other Ni-coordinating and bridging sulfur atoms. The electron density of the sulfur atom perpendicular to the Ni–S (Cys546) bond in *Dv*MF [NiFe] H_2ase exhibited an ellipsoid shape, supporting the hypothesis that the Ni-coordinating thiolate ligand of Cys546 is a proton acceptor.[24] We succeeded in simultaneously detecting two Ni-L states (Ni-L2 and Ni-L3) in *Dv*MF [NiFe] H_2ase by FT-IR and EPR measrements.[42] Both the Ni-L2 and Ni-L3 states were observed by light irradiation under basic conditions (pH 9.6 at 274 K), but the Ni-L3 state was not observed by light irradiation under mild basic conditions (pH 8.0 at 274 K). These results indicate that a residue, apparently Ni-coordinating Cys546, is protonated and deprotonated in the Ni-L2 and Ni-L3 states, respectively. The frequencies of the ν_{CO} and two ν_{CN} bands of the Ni-L3 state (ν_{CO}: 1890 cm^{-1}, ν_{CN}: 2034 and 2047 cm^{-1}) are 20 and 13–14 cm^{-1} lower than the corresponding frequencies of the Ni-L2 state (ν_{CO}: 1910 cm^{-1}, ν_{CN}: 2047 and 2061 cm^{-1}), respectively, at pH 9.6. The lower ν_{CO} and ν_{CN} frequencies of the Ni-L3 state compared to those of the Ni-L2 state are attributed to a stronger donor ability to the Ni ion for a thiolate compared to a thiol, leading to an increase in the electron density at the Ni^+–Fe^{2+} site with a metal–metal bond,[117] and thus a stronger π-back donation from the Fe ion to CO. Similar shifts to lower frequencies in the ν_{CO} bands (22–28 cm^{-1}) are observed for a [NiFe] model compound by the deprotonation of a terminal Ni-coordinating thiol.[125] The formation of two pH-dependent Ni-L states is also reported for *Pf* [NiFe] H_2ase, but the ν_{CO} frequency difference between the two Ni-L states was relatively small (5 cm^{-1}).[103] The small frequency difference is attributed to the isomerization of a protonated terminal Cys ligand,[69] where a nearby ionizable amino acid residue, creating a hydrogen bond with the Ni-coordinating Cys thiol and effectively preventing thiolate formation, is proposed.

A conserved Glu residue (Glu34 in the *Dv*MF sequence) located close to the Cys546 ligand is likely to be important for the proton transfer during the catalytic reaction according to structural, theoretical, and mutagenesis studies.[4,92,126,127] Greene *et al.* demonstrated that the Glu residue is a proton donor/acceptor for the interconversion between the Ni-C and Ni-SI_a states in *Pf* [NiFe] H_2ase using the E17Q mutant.[104] The structural perturbations of the Ni–Fe site by the E17Q mutation were small according to the FT-IR spectrum, which displayed ν_{CO} and ν_{CN} frequencies of the intermediates (Ni-SI_a, Ni-SI_r, Ni-C, and Ni-R states) similar to those in the wild-type enzyme spectrum. Time-resolved IR spectroscopic studies indicated that the E17Q mutation does not interfere with the bridging H^- photolysis, generating the two Ni-L states (Fig. 10).

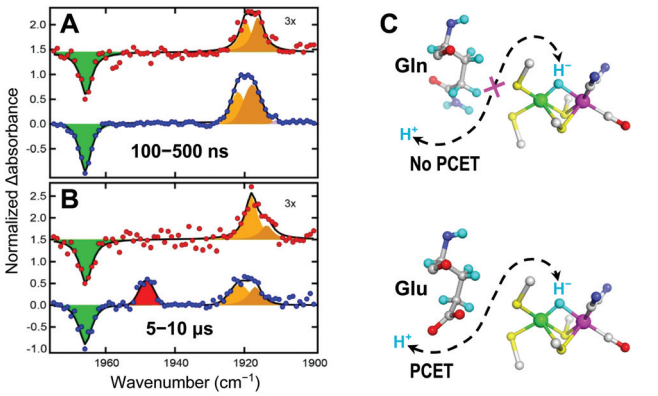

Fig. 10 (A, B) Normalized transient IR spectra of E17Q (red circles) and wild-type (blue circles) *Pf* [NiFe] H_2ase at pH 7.5 after 532 nm excitation and associated fit to the experimental data (black lines): (A) 100–500 ns and (B) 5–10 μs. Fit components are represented as shaded Voigt profiles for Ni-C (green), Ni-SI_a (red), and Ni-L (orange). (C) Proposed Glu gated PCET mechanism. Carbon, nitrogen, oxygen, sulphur, and iron atoms are shown in gray, blue, red, yellow, and pink spheres, respectively. Adapted with permission from ref. 104. Copyright 2016 American Chemical Society.

However, the E17Q mutation disrupted PCET from the Ni-L states to Ni-SI_a state, thereby preventing the formation of the Ni-SI_a state. Interestingly, all-atom MD simulations of *Aa* [NiFe] H_2ase revealed that the conformation of the side chain of the proton-accepting Glu residue (Glu13 in the *Aa* sequence) is flexible and adopts two orientations; 70% of the residues have the carboxylate side chain oriented toward the proximal Fe–S cluster, whereas 30% oriented toward the Ni–Fe site.[127] The conformational flexibility of the Glu residue may contribute to the proton transfer to and from the Ni–Fe site. Similar dual conformations of the Glu residue (Glu279) in the proton transfer pathway have been reported for [FeFe] H_2ase from *Clostridium pasterianum*.[128]

As discussed above, some important amino acids have been identified for the proton transfer between the Ni–Fe site and protein environment. However, the proton transfer pathways have yet to be fully understood, and are one of the major unsolved subjects for [NiFe] H_2ases.

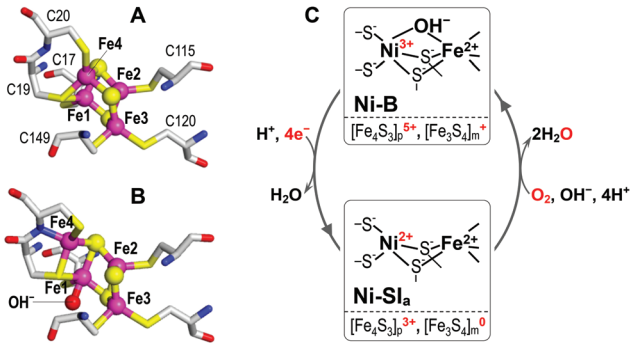

Fig. 11 (A, B) Structures of the proximal $[Fe_4S_3]$-6Cys cluster in the H_2-activated (A, PDB: 3RGW) and super-oxidized (B, PDB: 4IUB) states of O_2-tolerant *Re* [NiFe] H_2ase. Carbon, nitrogen, oxygen, sulphur, and iron atoms are shown in gray, blue, red, yellow, and pink spheres, respectively. (C) Proposed mechanism of O_2-inactivation and rapid activation for membrane-bound O_2-tolerant [NiFe] H_2ases.

Unique [NiFe] hydrogenases

The addition of an O_2-tolerant property to [NiFe] H_2ase, allowing [NiFe] H_2ases to maintain H_2 oxidation and/or H^+ reduction in the presence of O_2, may considerably increase the potential use of the enzyme for an energy storage medium.[6–9,129,130] Many crystal structures of unique O_2-tolerant [NiFe] H_2ases have been reported recently, providing new insights into the O_2-tolerant mechanisms of [NiFe] H_2ases.[131–135]

Membrane-bound O_2-tolerant [NiFe] hydrogenase

The Ni-A state found in O_2-sensitive [NiFe] H_2ases is absent in all O_2-tolerant [NiFe] H_2ases; the oxidized enzyme exists only in the Ni-B state as defined by EPR and FT-IR spectroscopy.[136,137] The crystal structures of O_2-tolerant [NiFe] H_2ases, including membrane-bound [NiFe] H_2ases from *Re*,[131,132] *Hydrogenovibrio marinus* (*Hm*),[133] and *Ec*,[134,135] have been solved recently. A unique proximal $[Fe_4S_3]_p$ cluster is found in these O_2-tolerant [NiFe] H_2ases, where six Cys residues (two extra Cys residues) are coordinated to the cluster (Fig. 11), whereas a $[Fe_4S_4]_p$ cubic cluster is located in standard [NiFe] H_2ases, where four Cys residues are coordinated to the cluster. In the H_2-activated state of *Re* [NiFe] H_2ase, four of the six Cys residues coordinate to the $[Fe_4S_3]_p$ cluster as in the cubic $[Fe_4S_4]_p$ cluster, one of the two extra Cys is coordinated as a terminal ligand to the $[Fe_4S_3]_p$ cluster, and the sulphur atom of the other extra Cys replaces one of the corner sulphides of $[Fe_4S_4]_p$ (Fig. 11A). In the super-oxidized $[Fe_4S_3]_p^{5+}$ state, the main chain amide nitrogen (Cys20 of *Re* [NiFe] H_2ase) is coordinated to Fe (termed Fe4) of the $[Fe_4S_3]_p$ cluster and stabilizes the super-oxidized state (Fig. 11B). Additionally, an OH^- ligand at Fe1 in the $[Fe_4S_3]_p$ cluster of *Re* [NiFe] H_2ase (Fig. 11B) and a carboxylate of Glu near Fe4 of the $[Fe_4S_3]_p$ clusters of *Hm* and *Ec* [NiFe] H_2ases may also stabilize the super-oxidized cluster. According to EPR and electrochemical measurements, the $[Fe_4S_3]_P$ cluster can exist in three oxidation states ($[Fe_4S_3]_P^{5+/4+/3+}$, E_m = +230 mV and +30 mV for *Ec* [NiFe] H_2ase).[122] The unusual $[Fe_4S_3]_P^{5+/4+/3+}$ with $[Fe_3S_4]_m^{+/0}$ may play a crucial role in the reduction of O_2 to H_2O,[138] preventing the formation of the Ni-A state (Fig. 11C);[122,131–134,138–141] the $[Fe_4S_3]_P$ cluster may donate two electrons to the Ni–Fe site, whereas the high potential medial $[Fe_3S_4]_m^{+/0}$ cluster (+190 mV for *Ec* [NiFe] H_2ase)[122] and the Ni ion (about 0 mV for Ni-SI_a (Ni^{2+}) and Ni-B (Ni^{3+}) for *Ec* [NiFe] H_2ase)[71] may provide one electron each, resulting in four electrons for O_2 reduction at the Ni–Fe site.

However, O_2-tolerant [NiFe] H_2ases from *Citrobacter sp.* S-77 [142–145] and *Pf*,[146] together with the O_2-tolerant V74C mutant[64,147] of the O_2-sensitive *Df* [NiFe] H_2ase, do not possess the unique $[Fe_4S_3]_p$ cluster, suggesting that other O_2-tolerant mechanisms may exist. For O_2-tolerant [NiFe] H_2ases possessing a $[Fe_4S_4]_p$ cluster, two mechanisms have been proposed. In the first mechanism, the electrocatalytic and EPR properties of *Pf* [NiFe] H_2ase are different from those of O_2-tolerant [NiFe] H_2ases possessing a $[Fe_4S_3]_p$ cluster, and thus, the electronic differences at the Ni–Fe site may play a role in the O_2-tolerance and formation of noncanonical inactive states in *Pf* [NiFe] H_2ase.[146] The O_2-tolerant V74C mutant of *Df* [NiFe] H_2ase exhibited similar electrochemical responses against H_2 and O_2, as well as in the presence of both H_2 and O_2, to those of *Pf* [NiFe] H_2ase.[146,147] The Ni–Fe site of the V74C mutant of *Df* [NiFe] H_2ase possesses an unusual structure in the Ni-coordination sphere. Instead of the coordination of four Cys thiolates to the Ni ion, two Cys thiolates, a bridging species (modeled as SH^-), and a main chain carboxy amido N atom are coordinated to the Ni ion.[64] The Ni–N(carboxamide) bond is hypothesized to stabilize the transient Ni^{3+}–OOH^- state with higher redox potential than that of the corresponding state of the wild-type enzyme, facilitating fast electron transfer and full O_2 reduction by the $[Fe_4S_4]_p$ and $[Fe_3S_4]_m$ clusters.[64,146] The second mechanism has been proposed for *Re* NAD^+-reducing [NiFe] H_2ase, where the sulfoxygenation of a bridging sulfur ligand plays a key role in the O_2 tolerance (*vide infra*).[148]

NAD$^+$-reducing [NiFe] hydrogenase

Soluble NAD$^+$-reducing [NiFe] H_2ase is another unique [NiFe] H_2ase. NAD$^+$-reducing [NiFe] H_2ase is a cytoplasmatic multi-subunit complex, comprising a heterodimeric [NiFe] H_2ase moiety (HoxH and HoxY) and a multimeric NAD$^+$ diaphorase module (HoxF and HoxU), which reduces NAD$^+$ to NADH.[2,6,129,149] *Re* NAD$^+$-reducing [NiFe] H_2ase contains a "standard" Ni–Fe site with one CO and two CN^- ligands coordinated to Fe according to *in situ* FT-IR and EPR spectroscopic studies of *Re* H16 cells.[113] Under *in vivo* conditions, 60% of the enzyme is found in the Ni-C state (g_x = 2.20, g_y = 2.14, g_z = 2.01), which photo-converts to the Ni-L state (g_x = 2.27, g_y = 2.10, g_z = 2.05) at 35 K. Multiple Ni-R states of *Re* NAD$^+$-reducing [NiFe] H_2ase were observed *in vivo* by FT-IR studies. Additionally, anaerobic as well as aerobic oxidation of the cell results in the formation of an EPR-silent "Ni-B-like" state. However, it is unclear whether the "Ni-B-like" state is the Ni-B (Ni^{3+}) state with the spin-coupling of the Ni center to other paramagnetic centers, or just a "Ni-B-like" (Ni^{2+}) state different from the Ni-B state.

Re NAD$^+$-reducing [NiFe] H_2ase generates superoxide, hydrogen peroxide, and water as catalytic by-products during H_2 oxidation in the presence of O_2.[150] Horch *et al.* explained the IR spectroscopic properties of *Re* NAD$^+$-reducing [NiFe] H_2ase with the Ni–Fe(CO)$(CN)_2$ site undergoing Cys sulfoxygenation in the "Ni-B-like" state (Fig. 12).[148] This sulfoxygenation is completely reversible, and thus may play a key role in the O_2 tolerance of the enzyme. The proposed mechanism fulfills the central criteria for the O_2-tolerant strategies in NAD$^+$-reducing [NiFe] H_2ases, namely (per)oxidase activity and the involvement of reversible oxidative modifications at the bridging Cys ligands. Similar mechanisms have been proposed for the O_2-tolerances of flavoprotein NADH peroxidase[151,152] and Ni model compounds.[153] Related to the reversible sulfoxygenation mechanism, Lindenmaier *et al.* reported the first sulfoxygenated heterobimetallic [NiFe] complex as a structural model for the sulfoxygenated active site of [NiFe] H_2ases.[154]

Shomura *et al.* reported the first X-ray crystal structures of NAD$^+$-reducing [NiFe] H_2ase from *Hydrogenophilus thermoluteolus* (*Ht*) TH-1 in the oxidized and reduced states (Fig. 13).[155]

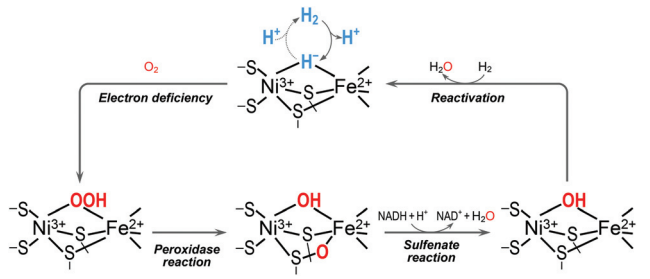

Fig. 12 Proposed O_2-tolerant mechanism for *Re* NAD$^+$-reducing [NiFe] H_2ase though the reversible sulfoxygenation of the Ni–Fe site. Adapted with permission from ref. 148. Copyright 2015 American Chemical Society.

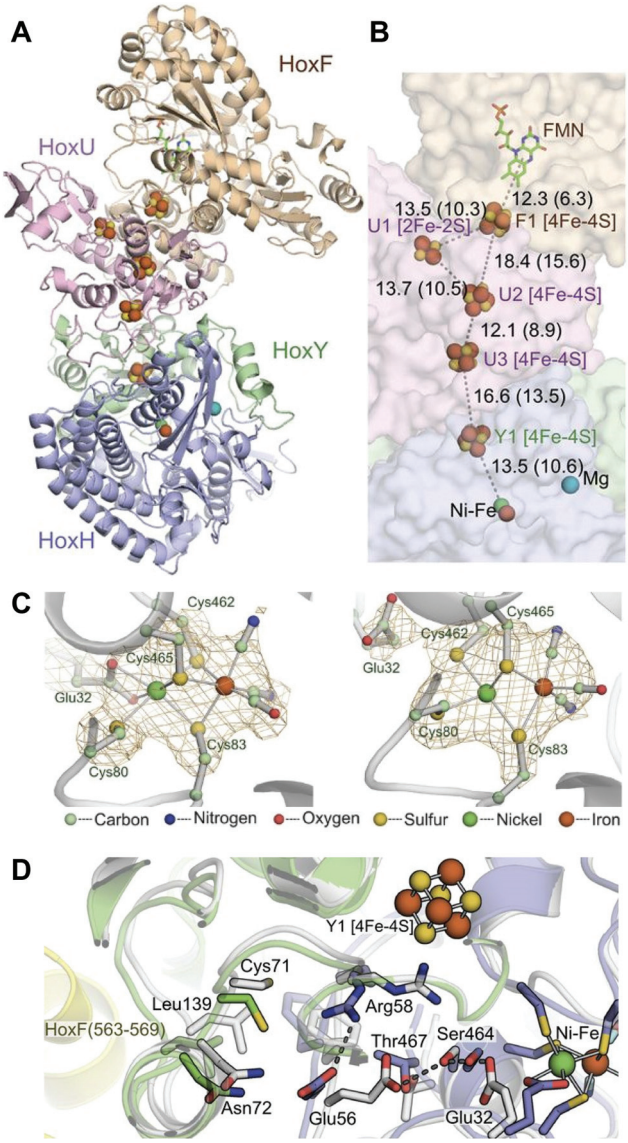

Fig. 13 Structure of *Ht* NAD$^+$-reducing [NiFe] H_2ase. (A, B) Overall structure and electron transfer pathway. (C) Ni–Fe site structures in the air-oxidized (left) and H_2-activated (right) states. (D) Structural determinant for the coordination of Glu32 to Ni. The atoms in the air-oxidized state are shown in the same colors as in A, and the H_2-activated state is shown in white. Adapted with permission from ref. 155. Copyright 2017 American Association for the Advancement of Science.

The five Fe–S cluster arrangement in the HoxY, HoxU, and HoxF subunits is similar to that of complex I from *Thermus thermophilus* HB8,[156,157] but the subunit orientation is not, which supports the hypothesis that the subunits of *Ht* NAD$^+$-reducing [NiFe] H_2ase and those of complex 1 have evolved independently and assembled as prebuilt modules into each energy metabolism machinery (Fig. 13A and B). The oxidized Ni–Fe site of *Ht* NAD$^+$-reducing [NiFe] H_2ase includes an unprecedented six-coordinate Ni geometry, which possesses a bidentate Ni-coordinating Glu ligand (Glu32 in the *Ht* sequence and Glu34 in the *Dv*MF sequence), a terminal Cys

ligand (Cys80), and three bridging Cys ligands (Cys83, Cys462, and Cys465) (Fig. 13C), and the coordination geometry would prevent O_2 from approaching the Ni–Fe site. In the reduced state, the normal Ni–Fe site structure was observed with the carboxy group of Glu32 uncoordinated to Ni and instead, the thiolate group of Cys462 coordinated as a terminal ligand to Ni. The conformational change was presumably triggered by the reduction/oxidation of the Y1-[Fe_4S_4] cluster near the Ni–Fe site (Fig. 13D). When activated, Glu32 in the hydrogen-bond network of Glu32–Ser464–Glu56 may be protonated and the guanidinium side chain of Arg58 oriented between the Glu56 side chain and the Y1-[Fe_4S_4] cluster, owing to a decrease in the charge of the Y1-[Fe_4S_4] cluster. However, when oxidized, the Ni–Fe site may be stabilized by the coordination of Glu32, and the carboxylate side chain of Glu56 forms a hydrogen bond with the guanidinium side chain of Arg58.

The air-oxidized *Ht* NAD^+-reducing [NiFe] H_2ase showed EPR signals (g_x = 2.25 and 2.26, g_y = 2.13, and g_z = 2.04) attributable to Ni^{3+}.[155] These results are in contrast to previous EPR results on other NAD^+-reducing [NiFe] H_2ases, in which no Ni-EPR signal was observed under various oxidized conditions.[6,129,149] However, the *g* values did not match those identified for the oxidized states of other [NiFe] H_2ases,[5,6] implying that the distinct configuration of the Ni–Fe site of the air-oxidized *Ht* NAD^+-reducing [NiFe] H_2ase is not an artifact caused by the crystallization. The EPR spectrum of the H_2-activated enzyme showed weak Ni-C state signals (g_x = 2.21 and g_y = 2.14; the g_z signal was overlapped with other signals), with *g* values close to those of the Ni-C state of *Re* NAD^+-reducing[113] and standard [NiFe] H_2ases,[5] supporting the idea that *Ht* NAD^+-reducing [NiFe] H_2ase adopts a normal Ni–Fe site configuration in the H_2-activated enzyme. Similar spectroscopic properties of the *Ht* NAD^+-reducing [NiFe] H_2ase have been reported by Preissler *et al.*[158] According to biochemical studies, *Ht* NAD^+-reducing [NiFe] H_2ase exhibits the highest H_2-mediated NAD^+-reduction activity at 80 °C (at pH 6.5), and its catalytic activity is sustained at low O_2 concentrations. Additional X-ray crystallographic studies of the *Ht* NAD^+-reducing [NiFe] H_2ase in the presence of NAD^+ and other NAD^+-reducing [NiFe] H_2ases may reveal the detailed O_2-tolerant mechanism.

Conclusions and outlook

While crystal structures and spectroscopic studies have provided significant insights into the [NiFe] H_2ase reaction mechanism, a number of important questions remain unanswered. We have investigated the acid–base equilibrium between the Ni-SI_r and Ni-SI_a states of [NiFe] H_2ase to elucidate the activation–inactivation mechanism.[40,65] Large activation energies and a large kinetic isotope (H/D) effect are obtained for the reconversion of the Ni-SI_a state to Ni-SI_r state, suggesting that the Ni–Fe site of the Ni-SI_a state reacts with a H_2O molecule and leaves a bridging OH^- ligand for the Ni-SI_r state. The precise structural determination on the Ni–Fe site of the Ni-SI_r and Ni-SI_a states requires further elucidation. The conserved Glu residue (Glu34 in the *Dv*MF sequence and Glu17 in the *Pf* sequence) may affect the proton and/or H_2O transfer in the equilibrium.[3,62] Future mutagenesis studies on the proton and H_2O transfer pathways may clarify the acid–base equilibrium mechanism.

Ogata *et al.* reported the ultrahigh resolution (0.89 Å) X-ray structure of the Ni-R state, where H^- at the Ni–Fe bridge and a protonated Ni-coordinating Cys546 ligand (*Dv*MF sequence) were observed, supporting Cys546 as an initial proton acceptor for the heterolytic cleavage of H_2.[24] The thiol-based H_2 cleavage mechanism has also been proposed through various model complexes and computational studies.[32,85,89–95] However, Armstrong and co-workers reported an alternative mechanism for the conversion of the Ni-SI_a state to Ni-R state: an Arg residue (Arg509 in the *Ec* sequence) proposed as the general proton accepting base for the H_2 cleavage.[86] For the conversion between the Ni-C and Ni-SI_a states, we,[42,70] Vincent and co-workers,[71] Armstrong and co-workers,[73] and Dyer and co-workers[72,103] demonstrated that the Ni-L state(s) is a catalytic cycle intermediate(s). Time-resolved spectroscopic studies reported by Dyer and co-workers indicated that the Cys and Glu residues (Cys379 and Glu17 in the *Pf* sequence, and Cys546 and Glu34 in the *Dv*MF sequence) are proton donors/acceptors in the Ni-SI_a ↔ Ni-C interconversion.[104] By comparing the PCET mechanism for the Ni-SI_a ↔ Ni-C transition (*via* Cys and Glu residues) and the PT mechanism for the Ni-SI_a ↔ Ni-R transition (*via* an Arg residue), both the Glu and Arg residues are strictly conserved and are necessary for the catalytic activity of [NiFe] H_2ases. However, there is no direct evidence for the proton transfer to both the Glu and Arg residues during the catalytic cycle reaction, and extended studies are necessary for the Ni-SI_a ↔ Ni-C and Ni-SI_a ↔ Ni-R transitions to be reconciled into a complete and comprehensive mechanism for H_2 activation and PT; in particular, isotope-label IR spectroscopic studies and neutron diffraction experiments on single crystals of the [NiFe] H_2ases may be useful.

The proton transfer pathway is also important for the effective functionalization of H_2 oxidation and production in [NiFe] H_2ases. The conserved Glu residue (Glu34 in the *Dv*MF sequence, Glu17 in the *Pf* sequence, and Glu32 in the *Ht* sequence) affects the proton transfer in the activation–inactivation and catalytic reactions. Glu34 in *Dv*MF [NiFe] H_2ase forms a relatively strong hydrogen bond (2.58 Å) with Thr18, which forms another low-barrier hydrogen bond[159] with Glu16 (2.62 Å), indicating the involvement of these residues in the proton transfer pathway.[24] Although knowledge on the proton transfer pathway is increasing, the proton transfer pathway is yet fully understood.

Shomura and co-workers reported the first oxidized and reduced crystal structures of an NAD^+-reducing [NiFe] H_2ase.[155] In the H_2-activated state, the Ni–Fe site exhibits the same ligand coordination structure as those of standard [NiFe] H_2ases. However, the air-oxidized Ni–Fe site possesses an unusual 6-coordinate Ni geometry. The air-oxidized enzyme

has an extra Ni-coordinating Glu ligand (Glu32 in the *Ht* sequence and Glu34 in the *Dv*MF sequence), preventing O_2 accession to the Ni–Fe center and protecting the Ni–Fe site against irreversible oxidation. However, various O_2-torelant [NiFe] hydrogenases with different Ni–Fe site and proximal Fe–S cluster structures exist. The clarification of the O_2-torelant mechanisms will yield productive results for understanding the reaction mechanisms of [NiFe] hydrogenases.

Further research in the mechanism elucidation of [NiFe] H_2ases by extended spectroscopic, X-ray and neutron crystallographic, electrochemical, and Ni–Fe site model compound studies will provide useful information for a future clean energy storage medium, especially for H_2 generation and biofuel cells.

Conflicts of interest

There are no conflicts to declare.

Acknowledgements

We are grateful to all co-workers and collaboration partners named in the cited references. We also acknowledge Mr Leigh McDowell, Nara Institute of Science and Technology, for his advice during manuscript preparation. This work was supported by the JST CREST (No. JPMJCR12M4 (Y. H. and S. H.)) and Grants-in-Aid for Scientific Research from JSPS (Young Scientists B, No. JP16K17936 (H. T.) and Scientific Research on Innovative Areas, No. JP15H00945 (S. H.)).

Notes and references

1 R. Cammack, M. Frey and R. Robson, *Hydrogen As a Fuel: Learning From Nature*, London and New York, 2001.
2 P. M. Vignais and B. Billoud, *Chem. Rev.*, 2007, **107**, 4206–4272.
3 A. L. De Lacey, V. M. Fernández, M. Rousset and R. Cammack, *Chem. Rev.*, 2007, **107**, 4304–4330.
4 J. C. Fontecilla-Camps, A. Volbeda, C. Cavazza and Y. Nicolet, *Chem. Rev.*, 2007, **107**, 4273–4303.
5 W. Lubitz, E. Reijerse and M. van Gastel, *Chem. Rev.*, 2007, **107**, 4331–4365.
6 W. Lubitz, H. Ogata, O. Rüdiger and E. Reijerse, *Chem. Rev.*, 2014, **114**, 4081–4148.
7 K. A. Vincent, A. Parkin and F. A. Armstrong, *Chem. Rev.*, 2007, **107**, 4366–4413.
8 J. A. Cracknell, K. A. Vincent and F. A. Armstrong, *Chem. Rev.*, 2008, **108**, 2439–2461.
9 F. A. Armstrong, N. A. Belsey, J. A. Cracknell, G. Goldet, A. Parkin, E. Reisner, K. A. Vincent and A. F. Wait, *Chem. Soc. Rev.*, 2009, **38**, 36–51.
10 S. Ogo, *Chem. Rec.*, 2014, **14**, 397–409.
11 A. Volbeda, M. H. Charon, C. Piras, E. C. Hatchikian, M. Frey and J. C. Fontecilla-Camps, *Nature*, 1995, **373**, 580–587.
12 J. W. Peters, W. N. Lanzilotta, B. J. Lemon and L. C. Seefeldt, *Science*, 1998, **282**, 1853–1858.
13 S. Shima, O. Pilak, S. Vogt, M. Schick, M. S. Stagni, W. Meyer-Klaucke, E. Warkentin, R. K. Thauer and U. Ermler, *Science*, 2008, **321**, 572–575.
14 S. Shima and R. K. Thauer, *Chem. Rec.*, 2007, **7**, 37–46.
15 R. K. Thauer, A. K. Kaster, M. Goenrich, M. Schick, T. Hiromoto and S. Shima, *Annu. Rev. Biochem.*, 2010, **79**, 507–536.
16 Y. Higuchi, T. Yagi and N. Yasuoka, *Structure*, 1997, **5**, 1671–1680.
17 Y. Montet, P. Amara, A. Volbeda, X. Vernede, E. C. Hatchikian, M. J. Field, M. Frey and J. C. FontecillaCamps, *Nat. Struct. Biol.*, 1997, **4**, 523–526.
18 P. M. Matias, C. M. Soares, L. M. Saraiva, R. Coelho, J. Morais, J. Le Gall and M. A. Carrondo, *J. Biol. Inorg. Chem.*, 2001, **6**, 63–81.
19 A. Volbeda, L. Martin, C. Cavazza, M. Matho, B. W. Faber, W. Roseboom, S. P. J. Albracht, E. Garcin, M. Rousset and J. C. Fontecilla-Camps, *J. Biol. Inorg. Chem.*, 2005, **10**, 239–249.
20 H. Ogata, P. Kellers and W. Lubitz, *J. Mol. Biol.*, 2010, **402**, 428–444.
21 Y. Higuchi, H. Ogata, K. Miki, N. Yasuoka and T. Yagi, *Structure*, 1999, **7**, 549–556.
22 H. Ogata, Y. Mizoguchi, N. Mizuno, K. Miki, S.-I. Adachi, N. Yasuoka, T. Yagi, O. Yamauchi, S. Hirota and Y. Higuchi, *J. Am. Chem. Soc.*, 2002, **124**, 11628–11635.
23 H. Ogata, S. Hirota, A. Nakahara, H. Komori, N. Shibata, T. Kato, K. Kano and Y. Higuchi, *Structure*, 2005, **13**, 1635–1642.
24 H. Ogata, K. Nishikawa and W. Lubitz, *Nature*, 2015, **520**, 571–574.
25 R. P. Happe, W. Roseboom, A. J. Pierik, S. P. J. Albracht and K. A. Bagley, *Nature*, 1997, **385**, 126.
26 A. J. Pierik, W. Roseboom, R. P. Happe, K. A. Bagley and S. P. J. Albracht, *J. Biol. Chem.*, 1999, **274**, 3331–3337.
27 T. Yagi, K. Kimura, H. Daidoji, F. Sakai and S. Tamura, *J. Biochem.*, 1976, **79**, 661–671.
28 V. H. Teixeira, C. M. Soares and A. M. Baptista, *Proteins*, 2008, **70**, 1010–1022.
29 I. F. Galván, A. Volbeda, J. C. Fontecilla-Camps and M. J. Field, *Proteins*, 2008, **73**, 195–203.
30 H. Ogata, W. Lubitz and Y. Higuchi, *Dalton Trans.*, 2009, 7577–7587.
31 C. Fichtner, C. Laurich, E. Bothe and W. Lubitz, *Biochemistry*, 2006, **45**, 9706–9716.
32 P. E. M. Siegbahn, J. W. Tye and M. B. Hall, *Chem. Rev.*, 2007, **107**, 4414–4435.
33 M. Bruschi, G. Zampella, P. Fantucci and L. De Gioia, *Coord. Chem. Rev.*, 2005, **249**, 1620–1640.

34 Y. Ohki and K. Tatsumi, *Eur. J. Inorg. Chem.*, 2011, **2011**, 973–985.
35 C. Tard and C. J. Pickett, *Chem. Rev.*, 2009, **109**, 2245–2274.
36 T. R. Simmons, G. Berggren, M. Bacchi, M. Fontecave and V. Artero, *Coord. Chem. Rev.*, 2014, **270**, 127–150.
37 S. Kaur-Ghumaan and M. Stein, *Dalton Trans.*, 2014, **43**, 9392–9405.
38 D. Schilter, J. M. Camara, M. T. Huynh, S. Hammes-Schiffer and T. B. Rauchfuss, *Chem. Rev.*, 2016, **116**, 8693–8749.
39 M. Y. Darensbourg, E. J. Lyon and J. J. Smee, *Coord. Chem. Rev.*, 2000, **206**, 533–561.
40 H. Tai, L. Xu, S. Inoue, K. Nishikawa, Y. Higuchi and S. Hirota, *Phys. Chem. Chem. Phys.*, 2016, **18**, 22025–22030.
41 M.-E. Pandelia, H. Ogata, L. J. Currell, M. Flores and W. Lubitz, *Biochim. Biophys. Acta*, 2010, **1797**, 304–313.
42 H. Tai, K. Nishikawa, S. Inoue, Y. Higuchi and S. Hirota, *J. Phys. Chem. B*, 2015, **119**, 13668–13674.
43 C. Fichtner, M. van Gastel and W. Lubitz, *Phys. Chem. Chem. Phys.*, 2003, **5**, 5507–5513.
44 V. M. Fernandez, E. C. Hatchikian and R. Cammack, *Biochim. Biophys. Acta*, 1985, **832**, 69–79.
45 S. Kurkin, S. J. George, R. N. F. Thorneley and S. P. J. Albracht, *Biochemistry*, 2004, **43**, 6820–6831.
46 S. E. Lamle, S. P. Albracht and F. A. Armstrong, *J. Am. Chem. Soc.*, 2004, **126**, 14899–14909.
47 M. Asso, B. Guigliarelli, T. Yagi and P. Bertrand, *Biochim. Biophys. Acta*, 1992, **1122**, 50–56.
48 D. Millo, M.-E. Pandelia, T. Utesch, N. Wisitruangsakul, M. A. Mroginski, W. Lubitz, P. Hildebrandt and I. Zebger, *J. Phys. Chem. B*, 2009, **113**, 15344–15351.
49 A. Volbeda, L. Martin, E. Barbier, O. Gutierrez-Sanz, A. L. De Lacey, P. P. Liebgott, S. Dementin, M. Rousset and J. Fontecilla-Camps, *J. Biol. Inorg. Chem.*, 2015, **20**, 11–22.
50 J. W. van der Zwaan, J. M. C. C. Coremans, E. C. M. Bouwens and S. P. J. Albracht, *Biochim. Biophys. Acta*, 1990, **1041**, 101–110.
51 M. Carepo, D. L. Tierney, C. D. Brondino, T. C. Yang, A. Pamplona, J. Telser, I. Moura, J. J. G. Moura and B. M. Hoffman, *J. Am. Chem. Soc.*, 2002, **124**, 281–286.
52 B. Bleijlevens, B. W. Faber and S. P. J. Albracht, *J. Biol. Inorg. Chem.*, 2001, **6**, 763–769.
53 M. van Gastel, C. Fichtner, F. Neese and W. Lubitz, *Biochem. Soc. Trans.*, 2005, **33**, 7–11.
54 M. van Gastel, M. Stein, M. Brecht, O. Schröder, F. Lendzian, R. Bittl, H. Ogata, Y. Higuchi and W. Lubitz, *J. Biol. Inorg. Chem.*, 2006, **11**, 41–51.
55 P. Amara, A. Volbeda, J. C. Fontecilla-Camps and M. J. Field, *J. Am. Chem. Soc.*, 1999, **121**, 4468–4477.
56 A. Pardo, A. L. De Lacey, V. M. Fernandez, Y. B. Fan and M. B. Hall, *J. Biol. Inorg. Chem.*, 2007, **12**, 751–760.
57 J. L. Barilone, H. Ogata, W. Lubitz and M. van Gastel, *Phys. Chem. Chem. Phys.*, 2015, **17**, 16204–16212.
58 A. L. de Lacey, E. C. Hatchikian, A. Volbeda, M. Frey, J. C. Fontecilla-Camps and V. M. Fernandez, *J. Am. Chem. Soc.*, 1997, **119**, 7181–7189.
59 B. Bleijlevens, F. A. van Broekhuizen, A. L. De Lacey, W. Roseboom, V. M. Fernandez and S. P. J. Albracht, *J. Biol. Inorg. Chem.*, 2004, **9**, 743–752.
60 S. E. Lamle, S. P. J. Albracht and F. A. Armstrong, *J. Am. Chem. Soc.*, 2005, **127**, 6595–6604.
61 S. J. George, S. Kurkin, R. N. F. Thorneley and S. P. J. Albracht, *Biochemistry*, 2004, **43**, 6808–6819.
62 A. L. De Lacey, A. Pardo, V. M. Fernandez, S. Dementin, G. Adryanczyk-Perrier, E. C. Hatchikian and M. Rousset, *J. Biol. Inorg. Chem.*, 2004, **9**, 636–642.
63 T. Krämer, M. Kamp, W. Lubitz, M. van Gastel and F. Neese, *ChemBioChem*, 2013, **14**, 1898–1905.
64 A. Volbeda, L. Martin, P. P. Liebgott, A. L. De Lacey and J. C. Fontecilla-Camps, *Metallomics*, 2015, **7**, 710–718.
65 H. Tai, L. Xu, K. Nishikawa, Y. Higuchi and S. Hirota, *Chem. Commun.*, 2017, **53**, 10444–10447.
66 R. P. Bell, *Chem. Soc. Rev.*, 1974, **3**, 513–544.
67 M.-E. Pandelia, H. Ogata, L. J. Currell, M. Flores and W. Lubitz, *J. Biol. Inorg. Chem.*, 2009, **14**, 1227–1241.
68 A. L. De Lacey, C. Stadler, V. M. Fernandez, E. C. Hatchikian, H. J. Fan, S. Li and M. B. Hall, *J. Biol. Inorg. Chem.*, 2002, **7**, 318–326.
69 A. Pardo, A. L. De Lacey, V. M. Fernández, H.-J. Fan, Y. Fan and M. B. Hall, *J. Biol. Inorg. Chem.*, 2006, **11**, 286–306.
70 H. Tai, K. Nishikawa, M. Suzuki, Y. Higuchi and S. Hirota, *Angew. Chem., Int. Ed.*, 2014, **53**, 13817–13820.
71 R. Hidalgo, P. A. Ash, A. J. Healy and K. A. Vincent, *Angew. Chem., Int. Ed.*, 2015, **54**, 7110–7113.
72 B. L. Greene, C. H. Wu, P. M. McTernan, M. W. Adams and R. B. Dyer, *J. Am. Chem. Soc.*, 2015, **137**, 4558–4566.
73 B. J. Murphy, R. Hidalgo, M. M. Roessler, R. M. Evans, P. A. Ash, W. K. Myers, K. A. Vincent and F. A. Armstrong, *J. Am. Chem. Soc.*, 2015, **137**, 8484–8489.
74 T. Yagi and Y. Higuchi, *Proc. Jpn. Acad., Ser. B*, 2013, **89**, 16–33.
75 K. A. Bagley, C. J. Van Garderen, M. Chen, E. C. Duin, S. P. J. Albracht and W. H. Woodruff, *Biochemistry*, 1994, **33**, 9229–9236.
76 L. M. Roberts and P. A. Lindahl, *J. Am. Chem. Soc.*, 1995, **117**, 2565–2572.
77 S. Ogo, K. Ichikawa, T. Kishima, T. Matsumoto, H. Nakai, K. Kusaka and T. Ohhara, *Science*, 2013, **339**, 682–684.
78 H. Ogata, T. Krämer, H. X. Wang, D. Schilter, V. Pelmenschikov, M. van Gastel, F. Neese, T. B. Rauchfuss, L. B. Gee, A. D. Scott, Y. Yoda, Y. Tanaka, W. Lubitz and S. P. Cramer, *Nat. Commun.*, 2015, **6**, 7890.
79 H. X. Wang, Y. Yoda, H. Ogata, Y. Tanaka and W. Lubitz, *J. Synchrotron Radiat.*, 2015, **22**, 1334–1344.
80 B. E. Barton and T. B. Rauchfuss, *J. Am. Chem. Soc.*, 2010, **132**, 14877–14885.
81 B. C. Manor and T. B. Rauchfuss, *J. Am. Chem. Soc.*, 2013, **135**, 11895–11900.

82 G. M. Chambers, M. T. Huynh, Y. L. Li, S. Hammes-Schiffer, T. B. Rauchfuss, E. Reijerse and W. Lubitz, *Inorg. Chem.*, 2016, **55**, 419–431.
83 O. A. Ulloa, M. T. Huynh, C. P. Richers, J. A. Bertke, M. J. Nilges, S. Hammes-Schiffer and T. B. Rauchfuss, *J. Am. Chem. Soc.*, 2016, **138**, 9234–9245.
84 L. C. Song, X. Y. Yang, M. Cao, X. Y. Gao, B. B. Liu, L. Zhu and F. Jiang, *Chem. Commun.*, 2017, **53**, 3818–3821.
85 H. Tang and M. B. Hall, *J. Am. Chem. Soc.*, 2017, **139**, 18065–18070.
86 R. M. Evans, E. J. Brooke, S. A. M. Wehlin, E. Nomerotskaia, F. Sargent, S. B. Carr, S. E. V. Phillips and F. A. Armstrong, *Nat. Chem. Biol.*, 2016, **12**, 46–50.
87 C. A. Fitch, G. Platzer, M. Okon, B. Garcia-Moreno and L. P. McIntosh, *Protein Sci.*, 2015, **24**, 752–761.
88 G. Berggren, A. Adamska, C. Lambertz, T. R. Simmons, J. Esselborn, M. Atta, S. Gambarelli, J. M. Mouesca, E. Reijerse, W. Lubitz, T. Happe, V. Artero and M. Fontecave, *Nature*, 2013, **499**, 66–69.
89 P. E. M. Siegbahn, *Adv. Inorg. Chem.*, 2004, **56**, 101–125.
90 M. Stein, E. van Lenthe, E. J. Baerends and W. Lubitz, *J. Am. Chem. Soc.*, 2001, **123**, 5839–5840.
91 M. Bruschi, M. Tiberti, A. Guerra and L. De Gioia, *J. Am. Chem. Soc.*, 2014, **136**, 1803–1814.
92 G. Dong and U. Ryde, *J. Biol. Inorg. Chem.*, 2016, **21**, 383–394.
93 S. Ding, P. Ghosh, A. M. Lunsford, N. Wang, N. Bhuvanesh, M. B. Hall and M. Y. Darensbourg, *J. Am. Chem. Soc.*, 2016, **138**, 12920–12927.
94 P. Ghosh, S. D. Ding, R. B. Chupik, M. Quiroz, C. H. Hsieh, N. Bhuvanesh, M. B. Hall and M. Y. Darensbourg, *Chem. Sci.*, 2017, **8**, 8291–8300.
95 S. D. Ding, P. Ghosh, M. Y. Darensbourg and M. B. Hall, *Proc. Natl. Acad. Sci. U. S. A.*, 2017, **114**, E9775–E9782.
96 C. L. Fan, M. Teixeira, J. Moura, I. Moura, B. H. Huynh, J. Legall, H. D. Peck and B. M. Hoffman, *J. Am. Chem. Soc.*, 1991, **113**, 20–24.
97 J. P. Whitehead, R. J. Gurbiel, C. Bagyinka, B. M. Hoffman and M. J. Maroney, *J. Am. Chem. Soc.*, 1993, **115**, 5629–5635.
98 M. Pavlov, P. E. M. Siegbahn, M. R. A. Blomberg and R. H. Crabtree, *J. Am. Chem. Soc.*, 1998, **120**, 548–555.
99 S. Q. Niu, L. M. Thomson and M. B. Hall, *J. Am. Chem. Soc.*, 1999, **121**, 4000–4007.
100 M. Stein and W. Lubitz, *Phys. Chem. Chem. Phys.*, 2001, **3**, 2668–2675.
101 S. Föerster, M. Stein, M. Brecht, H. Ogata, Y. Higuchi and W. Lubitz, *J. Am. Chem. Soc.*, 2003, **125**, 83–93.
102 M. Brecht, M. van Gastel, T. Buhrke, B. Friedrich and W. Lubitz, *J. Am. Chem. Soc.*, 2003, **125**, 13075–13083.
103 B. L. Greene, C. H. Wu, G. E. Vansuch, M. W. Adams and R. B. Dyer, *Biochemistry*, 2016, **55**, 1813–1825.
104 B. L. Greene, G. E. Vansuch, C. H. Wu, M. W. Adams and R. B. Dyer, *J. Am. Chem. Soc.*, 2016, **138**, 13013–13021.
105 B. L. Greene, G. E. Vansuch, B. C. Chica, M. W. W. Adams and R. B. Dyer, *Acc. Chem. Res.*, 2017, **50**, 2718–2726.
106 P. A. Ash, R. Hidalgo and K. A. Vincent, *ACS Catal.*, 2017, **7**, 2471–2485.
107 J. W. van der Zwaan, S. P. J. Albracht, R. D. Fontijn and E. C. Slater, *FEBS Lett.*, 1985, **179**, 271–277.
108 M. Medina, R. Williams, R. Cammack and E. C. Hatchikian, *J. Chem. Soc., Faraday Trans.*, 1994, **90**, 2921–2924.
109 M. Medina, E. C. Hatchikian and R. Cammack, *Biochim. Biophys. Acta*, 1996, **1275**, 227–236.
110 F. Dole, M. Medina, C. More, R. Cammack, P. Bertrand and B. Guigliarelli, *Biochemistry*, 1996, **35**, 16399–16406.
111 K. A. Bagley, E. C. Duin, W. Roseboom, S. P. J. Albracht and W. H. Woodruff, *Biochemistry*, 1995, **34**, 5527–5535.
112 P. Kellers, M.-E. Pandelia, L. J. Currell, H. Gorner and W. Lubitz, *Phys. Chem. Chem. Phys.*, 2009, **11**, 8680–8683.
113 M. Horch, L. Lauterbach, M. Saggu, P. Hildebrandt, F. Lendzian, R. Bittl, O. Lenz and I. Zebger, *Angew. Chem., Int. Ed.*, 2010, **49**, 8026–8029.
114 M.-E. Pandelia, P. Infossi, M. Stein, M.-T. Giudici-Orticoni and W. Lubitz, *Chem. Commun.*, 2012, **48**, 823–825.
115 E. Siebert, M. Horch, Y. Rippers, J. Fritsch, S. Frielingsdorf, O. Lenz, F. Velazquez Escobar, F. Siebert, L. Paasche, U. Kuhlmann, F. Lendzian, M.-A. Mroginski, I. Zebger and P. Hildebrandt, *Angew. Chem., Int. Ed.*, 2013, **52**, 5162–5165.
116 M. Horch, J. Schoknecht, M. A. Mroginski, O. Lenz, P. Hildebrandt and I. Zebger, *J. Am. Chem. Soc.*, 2014, **136**, 9870–9873.
117 M. Kampa, M.-E. Pandelia, W. Lubitz, M. van Gastel and F. Neese, *J. Am. Chem. Soc.*, 2013, **135**, 3915–3925.
118 P. A. Lindahl, *J. Inorg. Biochem.*, 2012, **106**, 172–178.
119 F. A. Armstrong, *Science*, 2013, **339**, 658–659.
120 D. Brazzolotto, M. Gennari, N. Queyriaux, T. R. Simmons, J. Pecaut, S. Demeshko, F. Meyer, M. Orio, V. Artero and C. Duboc, *Nat. Chem.*, 2016, **8**, 1054–1060.
121 K. Knuttel, K. Schneider, A. Erkens, W. Plass, A. Muller, E. Bill and A. X. Trautwein, *Bull. Pol. Acad. Sci., Chem.*, 1994, **42**, 495–511.
122 M. M. Roessler, R. M. Evans, R. A. Davies, J. Harmer and F. A. Armstrong, *J. Am. Chem. Soc.*, 2012, **134**, 15581–15594.
123 G. Dong, Q. M. Phung, S. D. Hallaert, K. Pierloot and U. Ryde, *Phys. Chem. Chem. Phys.*, 2017, **19**, 10590–10601.
124 G. Dong, U. Ryde, H. J. A. Jensen and E. D. Hedegård, *Phys. Chem. Chem. Phys.*, 2018, **20**, 794–801.
125 K. Weber, T. Krämer, H. S. Shafaat, T. Weyhermüller, E. Bill, M. van Gastel, F. Neese and W. Lubitz, *J. Am. Chem. Soc.*, 2012, **134**, 20745–20755.
126 S. Dementin, B. Burlat, A. L. De Lacey, A. Pardo, G. Adryanczyk-Perrier, B. Guigliarelli, V. M. Fernandez and M. Rousset, *J. Biol. Chem.*, 2004, **279**, 10508–10513.
127 F. Oteri, M. Baaden, E. Lojou and S. Sacquin-Mora, *J. Phys. Chem. B*, 2014, **118**, 13800–13811.
128 H. Long, P. W. King and C. H. Chang, *J. Phys. Chem. B*, 2014, **118**, 890–900.

129 H. S. Shafaat, O. Rudiger, H. Ogata and W. Lubitz, *Biochim. Biophys. Acta, Bioenerg.*, 2013, **1827**, 986–1002.
130 H. Ogata, W. Lubitz and Y. Higuchi, *J. Biochem.*, 2016, **160**, 251–258.
131 J. Fritsch, P. Scheerer, S. Frielingsdorf, S. Kroschinsky, B. Friedrich, O. Lenz and C. M. Spahn, *Nature*, 2011, **479**, 249–252.
132 S. Frielingsdorf, J. Fritsch, A. Schmidt, M. Hammer, J. Lowenstein, E. Siebert, V. Pelmenschikov, T. Jaenicke, J. Kalms, Y. Rippers, F. Lendzian, I. Zebger, C. Teutloff, M. Kaupp, R. Bittl, P. Hildebrandt, B. Friedrich, O. Lenz and P. Scheerer, *Nat. Chem. Biol.*, 2014, **10**, 378–385.
133 Y. Shomura, K. S. Yoon, H. Nishihara and Y. Higuchi, *Nature*, 2011, **479**, 253–256.
134 A. Volbeda, P. Amara, C. Darnault, J. M. Mouesca, A. Parkin, M. M. Roessler, F. A. Armstrong and J. C. Fontecilla-Camps, *Proc. Natl. Acad. Sci. U. S. A.*, 2012, **109**, 5305–5310.
135 A. Volbeda, C. Darnault, A. Parkin, F. Sargent, F. A. Armstrong and J. C. Fontecilla-Camps, *Structure*, 2013, **21**, 184–190.
136 M.-E. Pandelia, V. Fourmond, P. Tron-Infossi, E. Lojou, P. Bertrand, C. Leger, M. T. Giudici-Orticoni and W. Lubitz, *J. Am. Chem. Soc.*, 2010, **132**, 6991–7004.
137 M. Saggu, I. Zebger, M. Ludwig, O. Lenz, B. Friedrich, P. Hildebrandt and F. Lendzian, *J. Biol. Chem.*, 2009, **284**, 16264–16276.
138 P. Wulff, C. C. Day, F. Sargent and F. A. Armstrong, *Proc. Natl. Acad. Sci. U. S. A.*, 2014, **111**, 6606–6611.
139 T. Goris, A. F. Wait, M. Saggu, J. Fritsch, N. Heidary, M. Stein, I. Zebger, F. Lendzian, F. A. Armstrong, B. Friedrich and O. Lenz, *Nat. Chem. Biol.*, 2011, **7**, 310–318.
140 M.-E. Pandelia, D. Bykov, R. Izsak, P. Infossi, M. T. Giudici-Orticoni, E. Bill, F. Neese and W. Lubitz, *Proc. Natl. Acad. Sci. U. S. A.*, 2013, **110**, 483–488.
141 R. M. Evans, A. Parkin, M. M. Roessler, B. J. Murphy, H. Adamson, M. J. Lukey, F. Sargent, A. Volbeda, J. C. Fontecilla-Camps and F. A. Armstrong, *J. Am. Chem. Soc.*, 2013, **135**, 2694–2707.
142 S. Eguchi, K. S. Yoon and S. Ogo, *J. Biosci. Bioeng.*, 2012, **114**, 479–484.
143 N. T. Nguyen, T. Yatabe, K. S. Yoon and S. Ogo, *J. Biosci. Bioeng.*, 2014, **118**, 386–391.
144 T. Matsumoto, S. Eguchi, H. Nakai, T. Hibino, K. S. Yoon and S. Ogo, *Angew. Chem., Int. Ed.*, 2014, **53**, 8895–8898.
145 N. D. M. Noor, K. Nishikawa, H. Nishihara, K. S. Yoon, S. Ogo and Y. Higuchi, *Acta Crystallogr., Sect. F: Struct. Biol. Commun.*, 2016, **72**, 53–58.
146 P. Kwan, C. L. McIntosh, D. P. Jennings, R. C. Hopkins, S. K. Chandrayan, C. H. Wu, M. W. W. Adams and A. K. Jones, *J. Am. Chem. Soc.*, 2015, **137**, 13556–13565.
147 A. Abou Hamdan, P. P. Liebgott, V. Fourmond, O. Gutierrez-Sanz, A. L. De Lacey, P. Infossi, M. Rousset, S. Dementin and C. Leger, *Proc. Natl. Acad. Sci. U. S. A.*, 2012, **109**, 19916–19921.
148 M. Horch, L. Lauterbach, M. A. Mroginski, P. Hildebrandt, O. Lenz and I. Zebger, *J. Am. Chem. Soc.*, 2015, **137**, 2555–2564.
149 M. Horch, L. Lauterbach, O. Lenz, P. Hildebrandt and I. Zebger, *FEBS Lett.*, 2012, **586**, 545–556.
150 L. Lauterbach and O. Lenz, *J. Am. Chem. Soc.*, 2013, **135**, 17897–17905.
151 L. B. Poole and A. Claiborne, *J. Biol. Chem.*, 1989, **264**, 12330–12338.
152 J. I. Yeh, A. Claiborne and W. G. J. Hol, *Biochemistry*, 1996, **35**, 9951–9957.
153 M. Y. Darensbourg and W. Weigand, *Eur. J. Inorg. Chem.*, 2011, **2011**, 994–1004.
154 N. J. Lindenmaier, S. Wahlefeld, E. Bill, T. Szilvasi, C. Eberle, S. Yao, P. Hildebrandt, M. Horch, I. Zebger and M. Driess, *Angew. Chem., Int. Ed.*, 2017, **56**, 2208–2211.
155 Y. Shomura, M. Taketa, H. Nakashima, H. Tai, H. Nakagawa, Y. Ikeda, M. Ishii, Y. Igarashi, H. Nishihara, K. S. Yoon, S. Ogo, S. Hirota and Y. Higuchi, *Science*, 2017, **357**, 928–931.
156 L. A. Sazanov and P. Hinchliffe, *Science*, 2006, **311**, 1430–1436.
157 R. Baradaran, J. M. Berrisford, G. S. Minhas and L. A. Sazanov, *Nature*, 2013, **494**, 443–448.
158 J. Preissler, S. Wahlefeld, C. Lorent, C. Teutloff, M. Horch, L. Lauterbach, S. P. Cramer, I. Zebger and O. Lenz, *Biochim. Biophys. Acta*, 2017, **1859**, 8–18.
159 W. W. Cleland and M. M. Kreevoy, *Science*, 1994, **264**, 1887–1890.